Protein Science (1995), *4*:2203–2222. Cambridge University Press. Printed in the USA.

Molecular modeling studies of HIV-1 reverse transcriptase nonnucleoside inhibitors: Total energy of complexation as a predictor of drug placement and activity

MARILYN B. KROEGER SMITH,[1] CAROL A. ROUZER,[1,2] LISA A. TANEYHILL,[1,2] NATHAN A. SMITH,[2] STEPHEN H. HUGHES,[1] PAUL L. BOYER,[1] PAUL A.J. JANSSEN,[3] HENRI MOEREELS,[3] LUC KOYMANS,[3] EDWARD ARNOLD,[4] JIANPING DING,[4] KALYAN DAS,[4] WANYI ZHANG,[4] CHRISTOPHER J. MICHEJDA,[1] AND RICHARD H. SMITH, JR.[1,2]

[1] ABL-Basic Research Program, NCI-Frederick Cancer Research and Development Center, Frederick, Maryland 21702
[2] Department of Chemistry, Western Maryland College, Westminster, Maryland 21157
[3] Janssen Research Foundation, Turnhoutseweg 30, B-2340 Beerse, Belgium
[4] Center for Advanced Biotechnology and Medicine (CABM) and Chemistry Department, Rutgers University, 679 Hoes Lane, Piscataway, New Jersey 08854

(RECEIVED May 30, 1995; ACCEPTED July 25, 1995)

Abstract

Computer modeling studies have been carried out on three nonnucleoside inhibitors complexed with human immunodeficiency virus type 1 (HIV-1) reverse transcriptase (RT), using crystal coordinate data from a subset of the protein surrounding the binding pocket region. Results from the minimizations of solvated complexes of 2-cyclopropyl-4-methyl-5,11-dihydro-5*H*-dipyrido[3,2-*b* :2′,3′-*e*][1,4]diazepin-6-one (nevirapine), α-anilino-2,6-dibromophenylacetamide (α-APA), and 8-chloro-tetrahydro-imidazo(4,5,1-*jk*)(1,4)-benzodiazepin-2(*1*H)-thione (TIBO) show that all three inhibitors maintain a very similar conformational shape, roughly overlay each other in the binding pocket, and appear to function as π-electron donors to aromatic side-chain residues surrounding the pocket. However, side-chain residues adapt to each bound inhibitor in a highly specific manner, closing down around the surface of the drug to make tight van der Waals contacts. Consequently, the results from the calculated minimizations reveal that only when the inhibitors are modeled in a site constructed from coordinate data obtained from their particular RT complex can the calculated binding energies be relied upon to predict the correct orientation of the drug in the pocket. In the correct site, these binding energies correlate with EC_{50} values determined for all three inhibitors in our laboratory. Analysis of the components of the binding energy reveals that, for all three inhibitors, solvation of the drug is endothermic, but solvation of the protein is exothermic, and the sum favors complex formation. In general, the protein is energetically more stable and the drug less stable in their complexes as compared to the reactant conformations. For all three inhibitors, interaction with the protein in the complex is highly favorable. Interactions of the inhibitors with individual residues correlate with crystallographic and site-specific mutational data. π-Stacking interactions are important in binding and correlate with drug HOMO RHF/6-31G* energies. Modeling results are discussed with respect to the mechanism of complex formation and the design of nonnucleoside inhibitors that will be more effective against mutants of HIV-1 RT that are resistant to the currently available drugs.

Keywords: AIDS; binding energy; binding pocket; drug–protein interaction; HIV-1 reverse transcriptase; molecular modeling; nonnucleoside inhibitors

Reprint request to: Marilyn B. Kroeger Smith, ABL-Basic Research Program, NCI-Frederick Cancer Research and Development Center, P.O. Box B, Frederick, Maryland 21702; e-mail: kroeger@ncifcrf.gov.

Abbreviations: HIV-1, human immunodeficiency virus type 1; HIV-2, human immunodeficiency virus type 2; RT, reverse transcriptase; α-APA or 2,6-dibromo-α-APA, α-anilino-2,6-dibromophenylacetamide; TIBO or 8-chloroTIBO, 8-chloro-tetrahydro-imidazo(4,5,1-*jk*)(1,4)-benzodiazepin-2(*1*H)-thione; nevirapine, 2-cyclopropyl-4-methyl-5,11-dihydro-5*H*-dipyrido[3,2-*b* :2′,3′-*e*][1,4]diazepin-6-one; HEPT, 1-[(2-hydroxyethyl) methyl]-6-(phenylthio)thymine; *BE*, binding energy; RMS, root mean square deviation; HOMO, highest occupied molecular orbital; LUMO, lowest unoccupied molecular orbital.

The reverse transcriptase of HIV-1 has become an attractive target for drug design in the last few years. RT, which is virally encoded, is essential to the replication of HIV-1; it converts the viral RNA genome into a double-stranded linear DNA intermediate that is subsequently integrated into the host cell DNA (Goff, 1990; Mitsuya et al., 1990). HIV-1 RT consists of one 66-kDa polypeptide chain (p66), containing a polymerase domain and an RNase H domain, and one 51-kDa polypeptide chain (p51) containing only the polymerase domain (Dimarzo-Veronese et al., 1986). Two types of drugs that inhibit HIV-1 polymerase activity are nucleoside and nonnucleoside inhibitors. Although several members of the former class, such as 3′-azido-3′-deoxythymidine (AZT), 2′,3′-dideoxycytidine, and 2′,3′-dideoxyinosine, have shown promise in the clinic (Mitsuya et al., 1990; De Clercq, 1992), their usefulness is limited by toxicity and the emergence of drug-resistant mutants. In addition, these compounds appear to have undesirably broad specificity in that their 5′-triphosphate forms interact with other RTs, as well as with cellular DNA polymerases (Larder & Kemp, 1990; St. Clair et al., 1991; Larder, 1993; Richman, 1993; Schinazi, 1993; Tantillo et al., 1994).

Given the problems with nucleoside analogs, considerable effort has been expended in seeking alternatives. Much of the attention has been focused on the second class of drugs, collectively labeled "nonnucleoside inhibitors." Many classes of these agents have been reported in the last few years. Although they vary considerably in structure (Fig. 1), all of the drugs are highly specific for HIV-1; i.e., they do not inhibit a variety of other DNA polymerases including HIV-RT type 2. Although most of the drugs (such as nevirapine and the TIBO derivatives) appear to be mechanistically noncompetitive for primer, template, and nucleotide (Kopp et al., 1991; Romero et al., 1991), at least one inhibitor (HEPT) has been reported to be competitive with respect to the natural substrate dTTP (Baba et al., 1991). In addition, nonnucleoside inhibitors show a lower cellular toxicity than nucleoside inhibitors (Pauwels et al., 1990; Romero et al., 1991). Like the nucleoside drugs, however, the nonnucleoside inhibitors have been shown to induce the development of drug-resistant mutants. A number of studies have implicated the amino acid residues at positions 181 and 188, as well as at positions 100, 103, 106, 236, and to a lesser extent 98, 101, 108, 179, and 190, as being important in the development of resistance to the drugs (Nunberg et al., 1991; Mellors et al., 1992a and b; Balzarini et al., 1993; Pauwels et al., 1993; Richman, 1993; Tantillo et al., 1994).

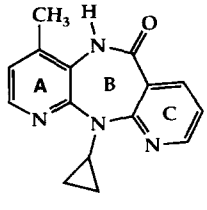

Nevirapine

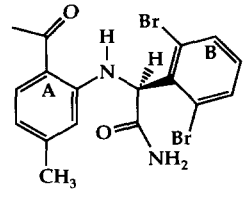

2,6-dibromo-α-APA

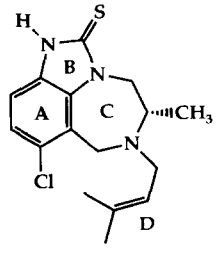

8-chloroTIBO

Fig. 1. Chemical structures of nevirapine, α-APA, and TIBO.

The results of mutational and crystallographic studies suggest that the majority of these compounds share a common binding site located near the RT polymerase active site. Inspection of the general structure of these nonnucleoside inhibitors reveals several common features. Each of the compounds is either constrained to or can adopt a conformation in which the compound assumes a "butterfly" shape (Ding et al., 1995a). Further, all of the compounds contain significant π-electron systems in the two "wing" sections of the molecules, defined as the portions of the inhibitor that lie either close to (wing I) or distal to (wing II) the polymerase active site (Ding et al., 1995a).

To date, the crystal structure of nevirapine complexed with RT has been published at moderate resolution (Kohlstaedt et al., 1992; Jäger et al., 1994; Smerdon et al., 1994) and, more recently, at higher resolution (Ren et al., 1995). Crystal structures for three additional inhibitors complexed with RT have been published: α-APA (Ding et al., 1995b; Ren et al., 1995), TIBO (Ding et al., 1995a), and HEPT (Ren et al., 1995). Furthermore, the structures of RT complexed with double-stranded DNA (Jacobo-Molina et al., 1993) and unliganded RT (Raag et al., 1994; Esnouf et al., 1995; Rodgers et al., 1995) have also been determined. The data from the crystallographic studies of RT-inhibitor complexes are in accord with the mutant data for each of the respective drugs.

In order to explore the common binding site for these various nonnucleoside inhibitors, we have undertaken molecular modeling studies of three drugs, nevirapine, α-APA, and TIBO (Fig. 1), using crystal structure coordinate data that were available at the time the study was initiated. The goals of this investigation were fourfold. First, we wished to determine if the drug orientation that was predicted to be best based upon total binding energy calculations matched that determined by crystallography. Second, we wanted to see if a particular set of RT/inhibitor coordinates could be used as a general template in the computer modeling of the binding of all of the inhibitors, or if each inhibitor needed to be modeled in a site derived from its own RT/inhibitor coordinates. Third, we wanted to determine if key side-chain residues around the binding pocket region differed significantly in orientation among the different inhibitor complexes. And finally, we wanted to determine and define the nature of the quantum mechanical component of potential π-stacking interactions between the inhibitors and the protein. Our long-term goal is to apply the information obtained in these calculations in the design of better nonnucleoside inhibitors.

Results and discussion

Overall computational conclusions

Affinity labeling studies with nevirapine (Palladino et al., 1994) suggest that the A ring of the inhibitor is oriented toward tyrosines 181 and 188 and the polymerase active site. This position has been confirmed by the determination of the crystal struc-

ture of the RT/nevirapine complex (Kohlstaedt et al., 1992; Smerdon et al., 1994; Ren et al., 1995). It has been suggested (Nanni et al., 1993; Ding et al., 1995b) that part of the interactions between nevirapine and RT, which help to orient the drug in the binding pocket, are due to π-stacking between the phenyl rings in the drug and the Y181 and Y188 aromatic side chains. An additional opportunity for π-stacking is provided by Y318/319 in the lower portion of the binding pocket, which is distal from the polymerase site.

Examination of the structure of the various drugs and those protein residues that constitute the binding pocket showed, for each inhibitor, that there are at least two orientations that permit extensive π-interaction, one of which corresponds to the position in the solved crystal structure (for description of orientations, see the Materials and methods). Our initial trial calculations of the inhibitors using the RT/nevirapine site showed the minimized geometry and attendant binding energy to be highly dependent upon the initial position of the drug in the binding pocket (for binding energy definition see the Materials and methods). In addition, HIV-1 RT seems to be relatively flexible in this region, and there appear to be a number of ways the protein side chains and backbone can shift to accommodate a drug in the binding pocket. As more crystallographic structural data became available for each of the inhibitors complexed with RT, this issue became more clearly resolved. We were then able to use, as a beginning point template, the proposed position of the drug in the crystal, admittedly with some degree of uncertainty given the 2.8–2.9 Å resolution of these data. Ultimately, a total of seven different orientations were modeled in the present study. In three of the orientations, the drug A ring was positioned toward Y181: (*R*)-nevirapine/A, α-APA/A, and TIBO-T2/A (sulfur toward β9 strand); in the remaining four orientations, the A ring of the drug was positioned down (toward Y318/Y319): (*R*)-nevirapine/C, α-APA/B, TIBO-T1/D (sulfur toward β10 strand), and TIBO-T2/D (sulfur toward β9 strand).

The results of the minimization calculations for the three inhibitors in various orientations and sites in the nonnucleoside binding pocket of RT are shown in Table 1. These data show that binding energies for any given inhibitor are most negative when the model uses coordinates based on the crystal data for the complex that contains that specific drug and RT. In addition, binding energies reliably predict the preferred orientation of a given drug in the binding pocket, if and only if the inhibitor is modeled in a site derived from the crystallographic data of the cognate complex. The optimal orientations of all three inhibitors, based on their respective best binding energy results, are completely in accord with the crystal structure determinations of their positions (Kohlstaedt et al., 1992; Smerdon et al., 1994; Ding et al., 1995a, 1995b; Ren et al., 1995). Protein backbone superposition of the final minimized positions of the three inhibitor complexes modeled in sites constructed from the corresponding coordinate data reveals that the drugs all roughly overlay each other in the RT binding pocket, maintaining a general "butterfly" shape (Fig. 2) with a protein RMS value of 1.3 Å. The greatest correspondence is seen for the portion of each drug that lies in the lower region of the binding pocket (toward Y318/319). Protein heavy atom superposition of the initial (crystal) and final minimized (preferred) orientations show that computed adjustments in the position of the drug and the protein reflect a further refinement of their crystal conformations (RMS: nevirapine-A, 0.596 Å; α-APA-A, 0.539 Å; and TIBO-T2/D, 0.556 Å). In general, these adjustments are within the accuracy limits of the crystallographic experiment. With one exception (TIBO-T2/A, 0.550 Å), the RMSs for the preferred orientation complexes were smaller than those of the other orientations tested (RMS: nevirapine-C, 0.620 Å; α-APA-B, 0.579 Å; and TIBO-T1/D, 0.557 Å).

The data in Table 1 further show that the calculated binding energies correlate with the measured EC_{50} values determined in this study, but only when a particular drug is modeled in a site constructed from the specific RT crystal coordinates of that complex. TIBO-T2/D was found to be the best inhibitor and its binding energy agreed with that assessment (EC_{50} = 0.31 μM, *BE* = −202 kcal/mol), followed in order by α-APA (EC_{50} =

Table 1. *Correlation of binding energy calculation results with various inhibitors in sites constructed from crystal structure coordinates with EC_{50} values*

	Binding energy (docking energy) (kcal/mol) in site			EC_{50} (μM) (with rCdG)	
Inhibitor/ring orientation to Y181	Steitz nevirapine	Arnold APA	Arnold TIBO	Literature	In-house
(*R*)-nevirapine/A[a,b]	−78 (−53)	n.d.	n.d.	0.084[c]	3.41
(*R*)-nevirapine/C	−24 (−43)	n.d.	n.d.		
APA/A[a,d]	+106 (−75)	−157 (−70)	n.d.	0.20[e]	0.42
APA/B	+80 (−65)	−144 (−59)	n.d.		
TIBO-T2/D[a,d]	−76 (−55)	−97 (−54)	−202 (−57)	0.34[f]	0.31[g]
TIBO-T1/D	−30 (−58)	−158 (−49)	−188 (−55)		
TIBO-T2/A	+79 (−49)	−105 (−50)	−130 (−53)		

[a] Boldfaced orientation corresponds to that reported in crystallographic analysis.
[b] Values are from calculations where Y319 was released in the 2nd and 3rd stages of the computer minimization procedure (see the Materials and methods).
[c] Taken from Hargrave et al. (1991).
[d] Values are from calculations where Y318 was released in the 2nd and 3rd stages of the computer minimization procedure (see the Materials and methods).
[e] Taken from Pauwels et al. (1993); assay performed on dichloro α-APA.
[f] Taken from Debyser et al. (1991); assay performed on TIBO (R82150).
[g] Assay carried out on 8-chloro TIBO (R86183).

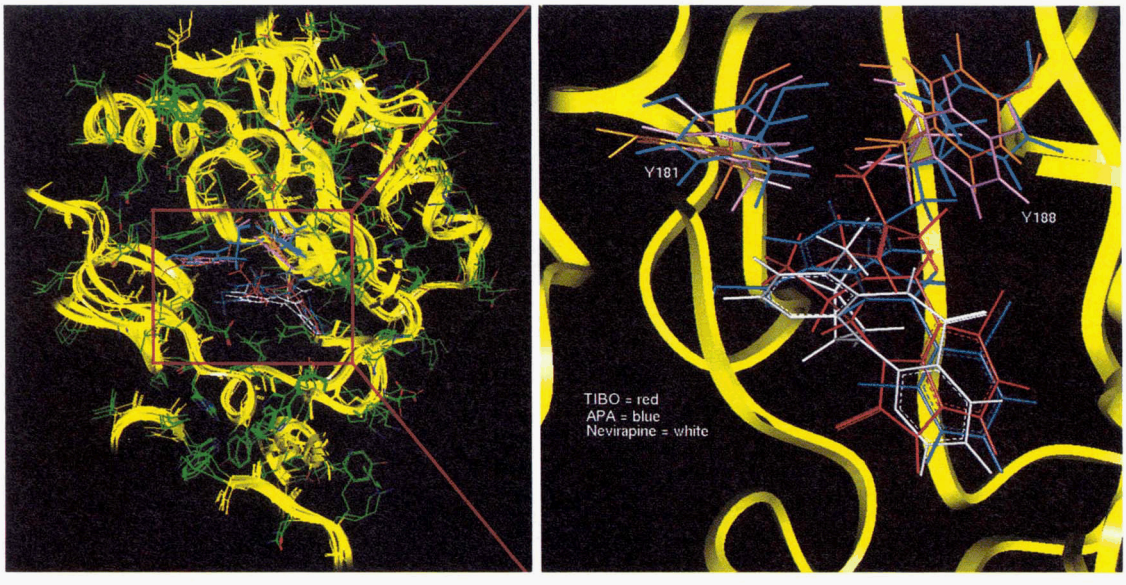

Fig. 2. Superposition by backbone of the minimized structures of α-APA, nevirapine, and TIBO complexed with RT in sites constructed from their own crystal structure coordinate data. α-APA is dark blue with its corresponding Y181, Y188, and W229 side-chain residues shown in light blue. Likewise, nevirapine is depicted in white, with its side chains in purple, and TIBO is shown in red, with its side chains in orange. The inset shows a close-up of the nonnucleoside inhibitor final orientations.

0.42 μM, $BE = -157$ kcal/mol) and nevirapine ($EC_{50} = 3.41$ μM, $BE = -78$ kcal/mol). The EC_{50} values, as measured for 8-chloro-TIBO and the dibromo analog of α-APA, are in reasonable agreement with published values for the closely related 9-chloroTIBO (0.7 μM), and dichloro analog of α-APA (0.1 μM), but differ markedly from the literature value for nevirapine (0.084 μM) (Debyser et al., 1991; Hargrave et al., 1991; Pauwels et al., 1993). At least some of these discrepancies may derive from the fact that substantially different assay conditions were used to obtain the various EC_{50} values. For example, in the nevirapine assay (Hargrave et al., 1991), an RT heterodimer at a concentration of 0.5 nM was used with a template-primer concentration of 0.8 mg/mL and a nucleotide concentration of 500 nM, whereas in both the TIBO (Debyser et al., 1991) and α-APA (Pauwels et al., 1993) assays, RT homodimer at 1 nM was used with a template-primer concentration of 40 mg/mL and a nucleotide concentration of 2.5 mM. In our assays, not only were template-primer and nucleotide concentrations different, but a much shorter incubation time (2 min) was employed. The rate of nucleotide incorporation (4.48 nM/s) was sufficiently high that 45% of available nucleotide would have been consumed in the 60-min assays. Such excessive consumption of substrate leads to a violation of steady-state conditions, in which it is assumed that the loss of substrate is minimal. The variations in observed EC_{50} values stress the importance of conducting assays under identical circumstances if potencies of different inhibitors are to be compared using the EC_{50} data.

Despite the considerable similarity in the positions of the three inhibitors in the binding pocket, there are key differences in the orientations of some of the side-chain residues surrounding the pocket; in particular, those of Y181, Y188, W229, Y318, Y319, F227, L234, and P95 derived from p66, and E138 derived from p51 (as discussed in the sections describing the binding of each drug). Among the different sites, the greatest variation in these residue orientations occurs in the upper region of the pocket (see Fig. 2), which corresponds to adjustment of the side chains to the larger differences in the positions of wing I as compared to wing II of the inhibitors. For each drug, these side chains adjust to make close van der Waals contact with the surface of the drug, excluding in the process waters initially associated with the solvated inhibitor. Only in the cases of nevirapine and α-APA does a remnant of these original waters of solvation remain in the complex. The interaction with W229 is especially notable, and the orientation of this conserved amino acid residue in the different sites is quite variable. The fact that there is a substantial difference in the positions of each of these residues in the final complex with different drugs further emphasizes the necessity of, and provides an explanation for, performing calculations using crystal structure coordinates specific to a particular inhibitor.

Aside from the variations between the various RT/α-APA, RT/nevirapine, and RT/TIBO sites, there are considerable differences between each of these complexes and either the RT/DNA or the unliganded RT starting sites. Overall, the RT/DNA site appears to be more similar to the sites in our minimized complexes than is the unliganded RT site. This is also true for the crystal structure data. For example, backbone superposition of the best α-APA complex with RT/DNA (RMS = 2.36 Å) can be compared with unliganded RT (2.79 Å). The principal differences appear to be in the positions of residues Y181, Y188, W229, and Y318.

At the present time, it is not known if the nonnucleoside inhibitors in this study form complexes with unliganded RT, RT/DNA, or both forms of the enzyme. However, as we have already noted, most nonnucleoside inhibitors are believed to be noncompetitive with respect to template-primer, suggesting that the inhibitor could bind both in the presence and absence of DNA. This idea is supported by recent biochemical experiments that suggest that, on the basis of kinetic analysis, DNA release

is not required for inhibitor binding (Spence et al., 1995). For this reason, our binding energy values were based on the minimized energy of the RT/DNA site, although the energy for the unliganded RT site was quite comparable (18 kcal/mol less stable). The use of a different starting structure and its attendant energy would alter all of the binding energies by a constant amount and hence would have no effect on their relative ordering (see the Materials and methods).

General theoretical observations

The ability of an inhibitor to complex with an enzyme, as reflected in the drug's EC_{50} and its thermodynamic counterpart, binding energy, is the consequence of a number of complex molecular interactions. Specifically, the calculated binding energy for the formation of an RT-drug complex involves changes in various intramolecular, intermolecular, and solvation energies associated with the reactants (the isolated drug and RT/DNA) and the product (drug bound to RT). For each drug, the largest favorable change observed is the result of an increase in solvation stabilization of the protein upon complexation (Table 2). This effect may be attributable to the general increase (8.5 ± 3.0%) in the surface area of the protein upon complexation and more than offsets an accompanying loss in solvation stabilization resulting from desolvation of the drug. In addition, formation of the drug-protein complex results in the development of favorable nonbonded interactions between the drug and the aromatic and nonaromatic protein residues that comprise the hydrophobic binding pocket. Conformational changes within the protein upon complexation also contribute in a substantially favorable fashion to the overall binding energy for α-APA and TIBO, but not nevirapine. Changes in the stability of the drug are relatively less important and are variable (α-APA is in a more favorable conformation, whereas nevirapine and TIBO are in less favorable conformations in the complex than alone in solvent).

In light of the preceding, it is not surprising that the drug-protein interaction energies, as measured by either $E_{interD'\text{-}P'}$ or final docking energy, do not correlate with EC_{50} values (see Tables 1, 2). On the basis of attractive forces between the drug and protein (Table 2), the most active drug should be α-APA, followed in order by TIBO and nevirapine. The EC_{50} values show instead TIBO > α-APA > nevirapine. Most published modeling studies of enzyme-inhibitor complexation reactions concentrate almost exclusively upon these interactions. For example, good correlations were recently obtained for a series of HIV-1 protease inhibitors following energy minimization in a totally rigid active site (Holloway et al., 1995). There is, however, no thermodynamic requirement that such a relationship should exist. In fact, our data in Table 2 demonstrate that, although drug-protein interactions influence the binding energy, they do not dominate the other contributing terms either in their absolute magnitude or in the variation among complexes. The distinction may lie in the fact that the inhibitor binding pocket of HIV-1 RT is quite flexible. Irrespective of this point, it is clear from our findings that, on both theoretical and practical grounds, drug-protein interaction energies are not necessarily a reliable predictor of EC_{50} values for drugs that have significantly different structures.

With this caveat in mind, it is still important to understand the nature of the protein-inhibitor interactions ($E_{interD'\text{-}P'}$) and to determine how these interactions contribute to the total binding energy of the drug in the pocket. This term consists of a combination of electrostatic, van der Waals, and aromatic stacking energies arising from interactions with surrounding protein residues. In the RT/inhibitor complexes in this study, hydrogen bonds between the protein and the inhibitor are important stabilizing interactions in the case of α-APA and TIBO, whereas drug-solvent hydrogen bonds are important for nevirapine binding. Contributions to inhibitor binding from electrostatic forces (see Table 3) are especially significant for residues Y188, K101, and K103, whereas van der Waals interactions with the drug are more important with residues L100, Y181, Y318/319, W229, V106, V179, G190, and L234.

Aromatic stacking interactions between the phenyl rings of the drugs and protein residues Y181, Y188, W229, and Y318/319 were observed for all three inhibitors (Table 4). The optimal distance between the aromatic rings has been reported (Burley & Petsko, 1985, 1988) to be in the range of 4.5-7.0 Å for all types of orientations, with an average separation distance of 5.5 Å. These interactions are usually of the favorable edge-to-face or offset stacked types (Hunter & Sanders, 1990; Hunter et al., 1991). In a more detailed investigation of such aromatic interactions, Jorgensen and Severance (1990) reported that the optimal centroid separation distance for the global minimum tilted T (edge-to-face) interaction is 4.99 Å, whereas that of the parallel stacked and displaced (offset stacked) interaction is 4.50 Å. The majority of the stacking interactions enumerated

Table 2. *Contribution to the total binding energy of the inhibitors from various component energies*

	Inhibitor						
	APA		Nevirapine		TIBO		
Energy (kcal/mol)	A	B	A	C	T2/D	T1/D	T2/A
Intradrug	−4.64	3.63	3.56	0.79	2.75	4.15	5.22
Intraprotein	−73.79	−48.67	35.96	73.48	−93.79	−52.34	−105.53
Interdrug-solvent	80.13	70.01	50.02	51.15	48.19	45.58	46.08
Interprotein-solvent	−96.57	−126.12	−119.50	−111.29	−107.70	−136.78	−29.38
Interdrug-protein	−62.70	−51.91	−47.69	−38.23	−51.18	−48.77	46.78
Total binding energy	−157.57	−144.06	−77.65	−24.10	−201.74	188.17	−130.39

Table 3. *Individual inhibitor-protein residue interaction energies (kcal/mol)*[a]

Drug/site	Y181	Y188	W229	Y319/318	L100	K101	K103	V106	V179	G190	L234
(*R*)-nevirapine/A[b]	**−4.45**	**−6.05***	−2.59	−2.25	−6.15	**−2.27***	**−6.73***	−3.42	−0.96	−1.23	−1.99
(*R*)-nevirapine/C[b]	−3.05	−5.90	**−4.08**	**−3.27**	−5.56	−0.66	+2.40	−2.08	−0.48	−0.70	−2.22
APA/A[c]	−6.35	**−10.16**	−3.27	−1.75	−5.83	**−3.04***	**−5.69***	−3.90	**−3.99**	−0.42	−2.90
APA/B[c]	−5.18	**−8.27***	−2.67	−1.73	−6.17	−0.40	**−1.67**	−3.65	−3.72	−1.30	−1.30
TIBO-T2/D[c]	−2.59	−6.71	−2.98	−1.56	−5.07	**−3.33***	**−2.57***	−3.44	−2.77	**−2.51**	**−3.37**
TIBO-T1/D[c]	−2.78	−4.25	−3.05	**−4.10**	−5.03	**−1.82***	**−4.28**	−2.72	−2.87	−1.81	−3.18
TIBO-T2/A[c]	−3.98	**−6.23**	**−4.32**	−0.99	−6.61	**−2.94**	−1.19	−1.63	−3.78	−1.35	−2.31

[a] Each energy is the sum of the van der Waals plus electrostatic energies. Boldface drug/site indicates orientation reported from crystallographic studies. Boldface value indicates contribution from electrostatic energy between 10 and 50% of total energy value shown. * Indicates contribution from electrostatic energy greater than 50% of total energy value shown.
[b] Interaction energies reported are from a minimization where Y319 is unconstrained in the latter two stages of the calculation.
[c] Interaction energies reported are from a minimization where Y318 is unconstrained in the latter two stages of the calculation.

Table 4. *Inhibitor-protein residue centroid distances*

Drug/site[a]	Residue	Distance (Å) A ring	Distance (Å) B,C, or D ring	Type of interaction
Nevirapine/A	Y181	5.01	9.84	Parallel displaced
	Y188	6.16	7.91	Tilted T
	W229[b]	6.80	9.47	Perpendicular T
	Y319[c]	8.56	5.30	Tilted T
Nevirapine/C	Y181	9.76	6.06	Parallel displaced
	Y188	8.36	4.08	Parallel displaced
	Y229	9.67	5.06	Tilted T
	Y319	5.95	9.08	Perpendicular T
APA/A	Y181	4.71	10.40	Parallel displaced
	Y188	5.32	7.95	Tilted T
	W229	5.66	10.06	Tilted T
	Y318[c]	6.66	4.98	Parallel displaced
APA/B	Y181	10.63	4.44	Parallel displaced
	Y188	8.34	6.39	Tilted T
	W229	10.31	5.96	Tilted T
	Y318[c]	5.04	7.21	Tilted T
TIBO-T2/D	Y181	10.35	6.23	Perpendicular T
	Y188	7.60	4.37	Parallel displaced
	W229	9.43	5.03	Parallel displaced
	Y318[c]	5.01	6.56	Tilted T
TIBO-T1/D	Y181	10.53	5.32	Perpendicular T
	Y188	8.97	5.11	Parallel displaced
	W229	9.96	5.39	Perpendicular T
	Y318[c]	4.78	6.9	Tilted T
TIBO-T2/A	Y181	5.27	8.92	Parallel displaced
	Y188	5.28	10.74	Tilted T
	W229	5.19	11.41	Perpendicular T
	Y318[c]	6.49	7.75	None

[a] For TIBO, the reported distance is between the aromatic ring of the side-chain residue and the double bond of the alkenyl side chain (ring D) of the drug. Boldface drug/site indicates orientation report from crystallographic studies.
[b] Centroid distances reported were calculated for all nine atoms in both rings of W229.
[c] Aromatic stacking was evaluated for Y319 in the case of nevirapine and Y318 in the cases of APA and TIBO. The orientations of Y319 and Y318 are roughly the same in the different sites (see the Materials and methods).

in Table 4 are somewhat less than ideal with respect to these optimal orientations of two π-stacked rings. Hence, we expect the contribution of π-stacking energy to the overall interaction energies listed in Table 4 to be less than the maximal value of ~2.0 kcal/mol per residue contacted (Jorgensen & Severance, 1990). It can be seen, however, that the measured interaction energies between the drug and these aromatic residues can be significantly greater than this. We attribute this difference to additional electrostatic and van der Waals interactions between the drug and the backbone and/or nonaromatic portions of these amino acid residues.

Although molecular mechanics, through van der Waals and electrostatic terms, accounts for much of the nonbonding interactions between properly oriented, proximate aromatic rings, it is also likely that there may be a significant quantum mechanical contribution to these interactions. One approach to evaluating this contribution is through frontier molecular orbital theory (Fukui & Fujimoto, 1967), a method that can be used to assess nonbonded π-interactions using a donor-acceptor model. Applying this model to our system, the drug can be viewed as acting either as a donor, giving up electrons from an occupied molecular orbital [generally that of highest energy (HOMO)], or as an acceptor, receiving electrons into an unoccupied molecular orbital [generally that of lowest energy (LUMO)]. The overlapping protein orbital would function as a corresponding acceptor or donor, respectively. The more favorable mode of drug action, donor or acceptor, would be that with the smallest energy difference ($\Delta E_{unocc-occ}$) between the involved pair of drug and protein molecular orbitals.

The locations and energies (Table 5) of the HOMO and LUMO molecular orbitals of each drug were determined using ab initio single point calculations on the drug geometry in the minimized complex. At the 6-31G* level, all of the occupied molecular orbitals had negative energies and all of the unoccupied orbitals had positive energies. The HOMO of nevirapine is located in the A ring (see Fig. 3), with the LUMO in the C ring. Likewise, the A ring of α-APA contains its HOMO, with the LUMO in the B ring. In TIBO, both the HOMO and LUMO are located across the A and B rings. The alkenyl side chain of TIBO is involved only in relatively less energetically favorable occupied (HOMO-3) and unoccupied (LUMO+5) orbitals.

Because of the variable influence of neighboring protein residues upon molecular orbital energies, it is not possible to use

Table 5. *HF molecular orbital energies*

	Energy in Hartrees[a] 3-21G* (6-31G*)	
Inhibitor/residue	HOMO	LUMO
Nevirapine	−0.29007 (−0.28754)	0.08744 (0.08888)
APA	−0.28909 (−0.28696)[b]	0.09092 (0.08845)[b]
TIBO-T1	−0.028536 (−0.28471)	0.10208 (0.10427)
TIBO-T2	−0.028455 (−0.28420)	0.10584 (0.10749)

[a] 1 Hartree = 627.5 kcal/mol

[b] HF/6-31G* energies calculated for APA are those for the analogous dichloro derivative of APA, adjusted by +0.00195 (HOMO) and −0.00091 (LUMO) based on 3-21G* molecular orbital energy differences for the dichloro and dibromo compounds.

a single generic tyrosine (or tryptophan) HOMO and LUMO energies to calculate the drug–protein donor–acceptor energy gap ($\Delta E_{unocc-occ}$). Nonetheless, AM1 semiempirical calculations on fragments mimicking the Y181, Y188, Y318/Y319, and W229 regions confirmed that appropriate molecular orbitals are located on the aromatic rings of these residues. These calculations showed, however, that the required orbitals differed among the various tyrosines and were not in all cases the most energetically favored HOMO and LUMO orbitals. The following exceptions were found: for the β9 fragment (180–182), the lowest unoccupied MO that involves the Y181 aromatic ring is the LUMO+1. For the β15 fragment (317–320), the LUMO involves Y319 and the LUMO+1 involves Y318. Occupied orbitals involving these same aromatic rings are unfavorably low lying, HOMO-5 for Y318 and HOMO-6 for Y319. From these results we can assume that a quantum mechanical component can contribute to π-stacking, but that such interactions can be expected to vary in importance, being least effective when Y318 or Y319 are acting as donors to a drug acceptor orbital. Thus, it appears that aromatic residues in the top of the pocket proximal to the active site can function as either donors or acceptors, but in the bottom of the pocket distal to the active site, they can serve only as potential acceptors.

From the preferred orientation of each of the drugs in the binding pocket, the location of the HOMO and LUMO of each drug, and the donor/acceptor capability of two regions of the binding pocket, it is possible to assign a donor/acceptor role to each of the inhibitors. Nevirapine and α-APA likely function as donors because their HOMO orbitals are oriented toward the top of the pocket where favorable protein-unoccupied orbitals are found. The α-APA and nevirapine LUMO orbitals extend toward the Y318/Y319 region, which is a relatively poor donor. TIBO is probably also a donor in that both its HOMO and LUMO are positioned in the Y318/Y319 region, which has unfavorable donor characteristics. In their role as electron donors, examination of the magnitude of the HOMO energies for all

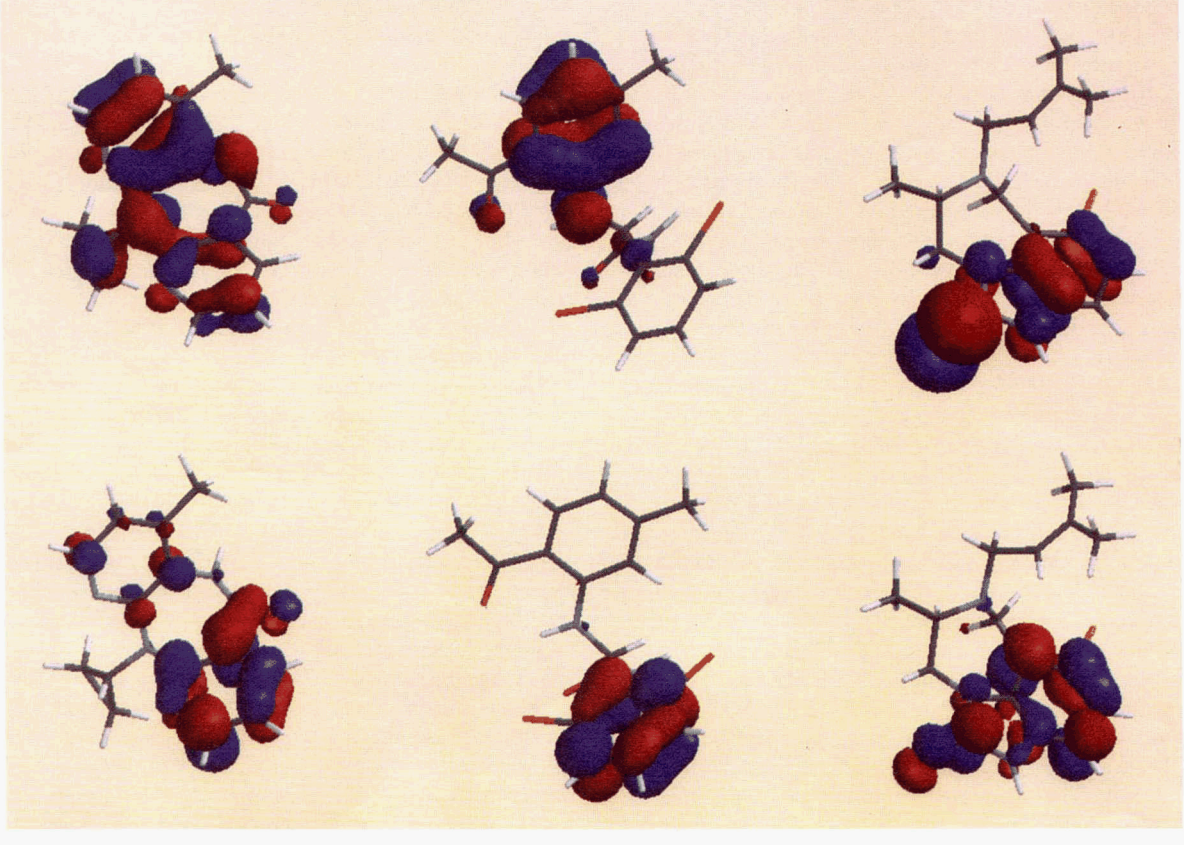

Fig. 3. Locations of the highest occupied (HOMO) (top row) and lowest unoccupied (LUMO) (bottom row) molecular orbitals in nevirapine, α-APA, and TIBO, left to right, respectively. Calculations were performed and visualized using the program Spartan.

three drugs (Table 5) predicts TIBO-T2 to be a better drug (less negative energy) than TIBO-T1, followed in order by α-APA and nevirapine. Despite the relatively small contribution that such interactions may make in the binding of the inhibitors, it is intriguing that the order of these energies correlates with the total binding energy and EC_{50} data.

Discussion of results from modeling each inhibitor

Nevirapine

Nevirapine (BI-RG-587) is a chiral molecule; therefore, there are two conformations, *R* and *S*, of the drug. Surprisingly, a crystal structure determination of nevirapine itself (Schafer et al., 1993) reported only the *R* isomer (possibly an oversight) and this was the conformation in the crystal structure of the RT/nevirapine complex (Kohlstaedt et al., 1992; Smerdon et al., 1994; Ren et al., 1995). The results from the modeling calculations, constructed from a site derived from RT/nevirapine coordinate data (Smerdon et al., 1994), are shown in Table 1. In addition to the orientation with the A ring positioned toward Y181 (designated as (*R*)-nevirapine/A), we also modeled (*R*)-nevirapine/C, which has the cyclopropyl ring facing B10 instead of B9. This latter position has a substantially higher binding energy (by 54 kcal/mol) than the orientation in the crystal structure. In addition, it also has a worse final docking energy (−43 versus −53 kcal/mol).

In the A orientation, backbone superposition of the initial (reported crystal geometry) and final (molecular mechanics minimized geometry) structures of the complex gave an RMS = 0.45 Å, with movement of nevirapine during the minimization of ~1 Å down from W229. The (*R*)-nevirapine/A minimized model shows no hydrogen bonds between the drug and the protein, in agreement with crystal structure data (Kohlstaedt et al., 1992; Smerdon et al., 1994; Ren et al., 1995). In the minimized complex, there are two hydrogen bonds from the C ring N10 of nevirapine to one solvent molecule and one hydrogen bond from the nevirapine A ring N1 to a second solvent molecule, in agreement with recent published data (Ren et al., 1995). These waters bridge to protein residues E138 in p51 and K103 in p66, respectively, which are located at the entrance to the binding pocket. Ren et al. (1995) also observed one additional hydrogen bond from the carbonyl oxygen atom to solvent, which we did not see in our model. The crystal data used in developing our model (Smerdon et al., 1994) were not of sufficient resolution to show specific water molecules in the pocket.

The contributions to the total binding energy by each of the interactions accompanying complex formation are summarized in Table 2. It can be seen that the largest favorable contribution is from intermolecular protein-solvent interactions, followed by intermolecular drug-protein interactions. The former effect is more pronounced in the case of the RT/nevirapine complex than it is for either of the other drugs. Substantial stabilization (−47.69 kcal/mol) derives from drug-protein interactions, reflecting the "shrink-wrap" of the protein side chains around the drug (see Fig. 4). The value for the intermolecular drug-protein energy contribution from our calculations is close to the final docking energy of the drug (−53 kcal/mol). It is, however, more negative than that for nevirapine/C (−38 kcal/mol) and agrees with the fact that with the A orientation of the inhibitor is favored. The remaining energy terms, intramolecular energy changes within the drug and the protein, and intermolecular drug-solvent interaction, all disfavor the formation of the complex. Nevirapine exists in a slightly less stable (by 3.56 kcal/mol) conformation when present in the complex. In contrast to the other inhibitors, the stability of the protein upon complexation with nevirapine is significantly reduced. The specific source of this destabilization has not been determined.

The major side-chain residues that show significant movement as the reaction proceeds from the RT/DNA structure to the final minimized complex are Y181, Y188, and W229. Comparison of the W229 orientation in RT/nevirapine to that in RT/DNA (or unliganded RT) reveals that it is rotated 180° and displaced by 4.2 (or 4.3 Å). The motion of W229 allows the aromatic side chains of Y181 and Y188 to rotate upward (by 81° and 107°, respectively, compared to RT/DNA; by 129° and 119°, respectively, compared to unliganded RT), vacating the region in which the drug will reside (see later discussion on the mechanism of inhibitor binding). Taken together, these motions permit the inhibitor to enter and bind in the newly created pocket, with subsequent adjustment of the side chains of P95, L100, K101, K103, V106, V179, G190, F227, L234, and Y319 from p66 and E138 from the p51 subunit.

The minimized structure of RT/nevirapine shows substantial intermolecular interactions between the drug and several amino acid residues: K103, Y188, L100, Y181, V106, and K101. The contribution of each of these interactions to the total binding energy is given in Table 3. These six residues alone account for 61% of the total drug-protein interaction energy. Electrostatic contributions are a major component of the K101 and K103 binding energies and a minor part of the Y181 and Y188 binding energies. The alternative nevirapine orientation (C ring to Y181) shows contributions from residues Y188, L100, W229, Y319, and Y181, with electrostatic energy from residues W229 and Y319 being a minor contributor to the total energy. There is, however, no significant stabilizing interaction with K101 or K103 in the alternative orientation. Clearly this is a significant contributing factor in explaining why the nevirapine/C orientation is not the preferred position for the inhibitor. For each of the residues mentioned above, the magnitude of the interaction energy is greater in the preferred orientation than in the alternative position.

The interaction with L100 and V106, two nonaromatic hydrophobic residues, is also significant. L100 in particular plays an important role in defining the "butterfly" shape of the pocket, lying in the concave face of the drug. Contact of L100 with both wings of the drug leads to a substantial stabilizing interaction energy (−6.15 kcal/mol); only K103 makes a larger contribution. V106 contacts only the convex face of the C wing and consequently has a smaller, but still important, stabilizing influence.

Aromatic stacking was observed in the optimal nevirapine-minimized orientation, with centroid to centroid distances generally in the range of 5–6 Å (see Table 4). The interactions observed are of the more favorable parallel displaced and T types, which correspond to those observed in the crystal structure (Kohlstaedt et al., 1992; Smerdon et al., 1994; Ren et al., 1995). The orientation with the A ring toward Y181 has a more favorable separation distance for this aromatic interaction than does the alternative C position (5.01 versus 6.06 Å). Tilted T stacks in the A orientation were observed with Y188 and Y319, whereas a perpendicular T can be seen to W229. It is clear from the interaction energies (Table 3) that con-

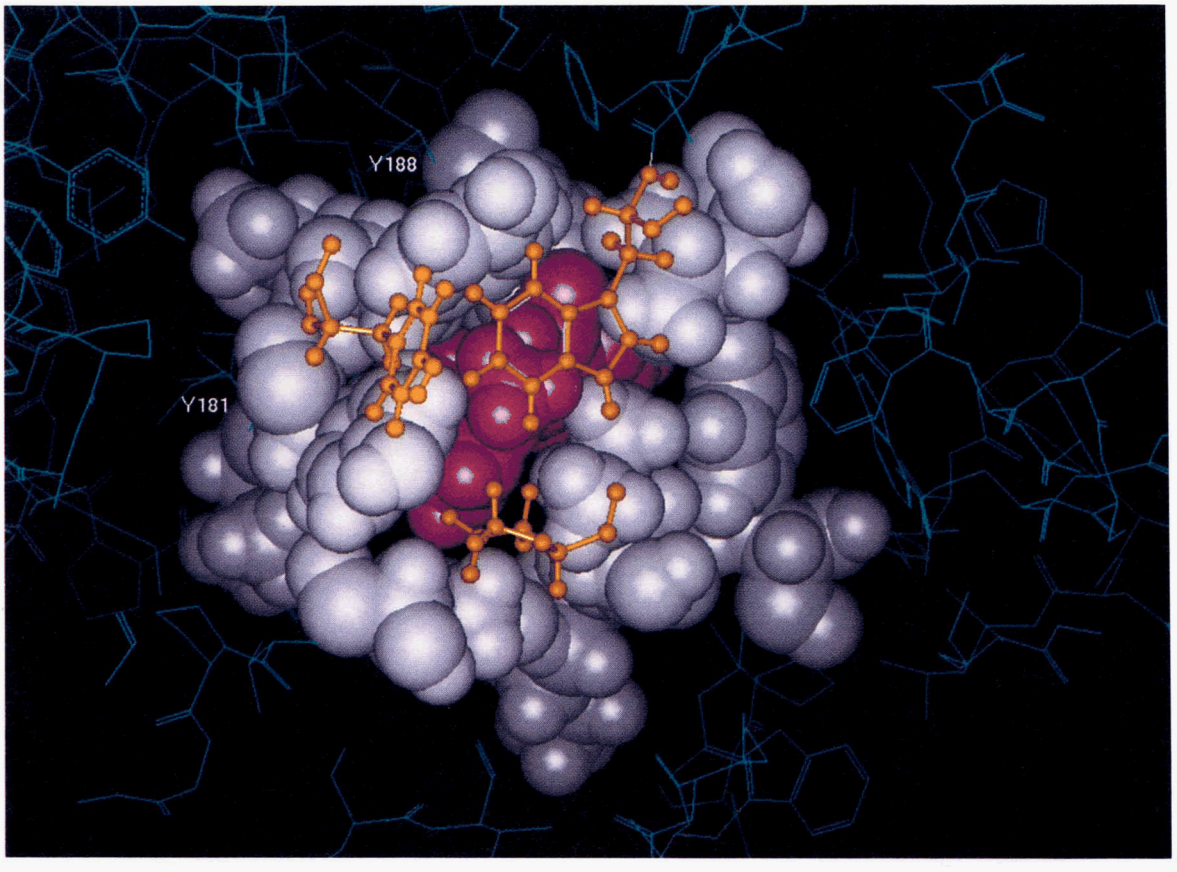

Fig. 4. Close-up view of the nevirapine binding pocket, with a space-filling model of the drug shown in purple. The van der Waals surface of the key side-chain residues surrounding the pocket are depicted in orange and white. White residues in the plane of the inhibitor are shown as white solids, and orange ball-and-stick residues (W229, Y183, and P95) project out of the plane.

tacts with Y181 and Y188 are more important than those with the other aromatic residues.

The significance of both Y181 and Y188 (as well as K103) to the binding of nevirapine has been dramatically shown in mutagenesis experiments (Nunberg et al., 1991; Richman et al., 1991; Larder, 1992; Mellors et al., 1992a and b; Sardana et al., 1992; Schleif et al., 1992; Bacolla et al., 1993; Balzarini et al., 1993; Debyser et al., 1993). The conservative substitutions of Y181F or Y188F only slightly decreased inhibition by nevirapine, whereas the more radical substitution of isoleucine or cysteine for Y181 or Y188, respectively, resulted in an enzyme that was resistant to nevirapine. This supports the hypothesis that these π-stacking interactions are crucial. Replacement of either Y318 or Y319 with leucine had no effect on the ability of nevirapine to inhibit (P.L. Boyer & S.H. Hughes, unpubl. data), which correlates with the lack of aromatic stacking with this residue. W229 is necessary for RT activity (Boyer & Hughes, unpubl. data; Jacques et al., 1994) and thus its role in drug binding cannot be assessed through mutation experiments. Further, the substitution of asparagine for lysine at residue 103 resulted in only a slight change in the enzyme's sensitivity to nevirapine. This is at first somewhat surprising given the importance of electrostatic forces in the interaction with this residue. It is clear from our minimized structure, however, that important contacts are made between the hydrocarbon portions of the K103 side chain (especially CB, CG, and CE) with the C wing and cyclopropyl group of nevirapine. These contacts would be reduced, but not totally removed, by the K103N mutation.

α-APA

The conformation of α-APA (R95845) taken from crystal structure data (Ding et al., 1995b) was minimized both in a site constructed from RT/α-APA coordinates and in a site made from RT/nevirapine coordinates. Table 1 shows that the binding energies are much better for α-APA in its own site than in a site constructed from RT/nevirapine coordinates (-157 versus $+106$ kcal/mol). If the RT/α-APA site is used in the calculation, our binding energy data (Table 1) show α-APA/A to be the correct orientation and the crystal structure data agree with this conclusion (Ding et al., 1995a, 1995b; Ren et al., 1995). Use of the RT/nevirapine site leads to incorrect results in predicting the correct orientation of α-APA.

The overall RMS of the backbone superimposed initial and final configurations was 0.42 Å. This value is similar to that measured in the nevirapine minimization and is consistent with the level of uncertainty associated with crystal structures of resolution 2.8–2.9 Å. The drug was found to move about 0.7 Å during the minimization, with the largest change being rotation of the carboxamido group ~90° from its starting (crystal structure) orientation (Ding et al., 1995b). In the minimized structures of

α-APA, modeled in their own coordinate site, the carboxamido N-*H* of α-APA was found to interact with the backbone carbonyl oxygen of Y188. The geometry of this interaction, however, is beyond the bounds of normal hydrogen bonds between an N-*H* and a carbonyl oxygen (Taylor et al., 1985). The N–O distance is 3.06 Å, the H–O distance is 2.39 Å, the H–O–C angle is 108°, and the hydrogen atom lies 72° out of the plane of the carbonyl group. We also observed a weak interaction of the same type with the backbone carbonyl of V179 (N–O distance = 3.63 Å, H–O distance = 2.79 Å, with the H–O–C angle = 108°), as was recently reported in a second crystal structure determination (Ren et al., 1995). In the crystal structure of Ding et al., potential hydrogen bonding interactions between the carboxamido N-*H* of α-APA and the backbone carbonyl oxygens of Y188 and V189 are reported. It appears our further refinement of the crystal structure alters the position of the α-APA carboxamido group enough to change its potential interactions with the various nearby backbone carbonyl oxygen atoms. In addition, one hydrogen bond from the acetyl oxygen (O1B) of α-APA to a solvent molecule was observed, in agreement with crystal data (Ding et al 1995a; Ren et al., 1995). Further, this same water molecule also hydrogen bonds to the carboxylate oxygen of E138 in p51.

The contributions to the total binding energy by each of the interaction energy changes accompanying complex formation are summarized in Table 2. The intermolecular protein–solvent energy is the most important contributor to the binding energy, followed by the intramolecular energy of the protein and the intermolecular drug–protein interaction. As is true for each of the complexes that we have studied, the protein experiences increased stabilization from the solvent upon complexation. Unlike the nevirapine case, the protein in the α-APA complex is in a significantly more stable conformation when complexed with the drug. As with both other inhibitors, drug–protein interactions play an important role in favoring the formation of a complex. The drug–protein interaction energy for the A orientation (−63 kcal/mol) is close to the final docking energy (−70 kcal/mol) and is more favorable than for the alternative B position. Substantial stabilization is derived from the close fit of the van der Waals surfaces of the drug and the protein residues in the binding pocket (Fig. 5). α-APA is the only drug that exists in a more stable conformation ($\Delta E_{intradrug} = -4.64$ kcal/mol) in the complex as compared to that in solvent. The sole unfavorable term in the binding energy equation is that associated with desolvation of the drug upon complexation with RT. Among the three drugs, this term is largest for α-APA. This loss of solvation energy is reasonable given the presence of three potential hydrogen bonding moieties (amino, carboxamido, and acetyl) in the drug and an average of four hydrogen bonds to solvent in the uncomplexed drug, compared with one to the ace-

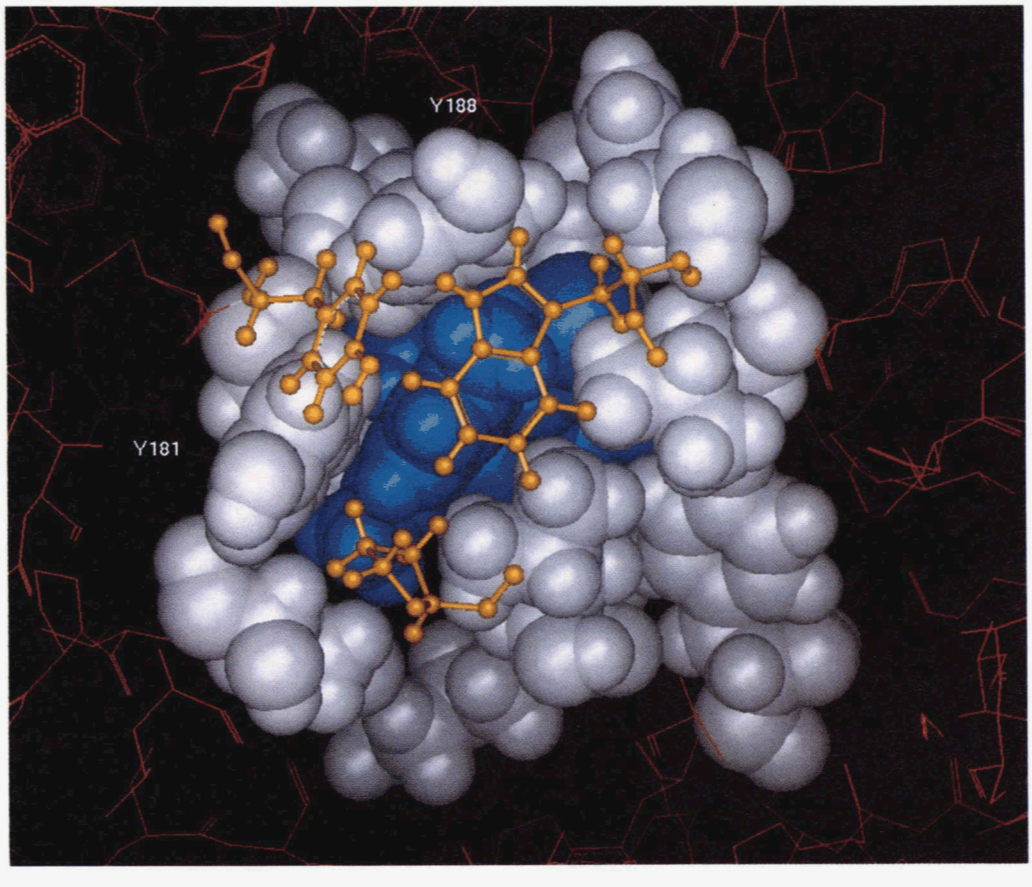

Fig. 5. Close-up view of the α-APA binding pocket, with a space-filling model of the drug shown in blue. The van der Waals surface of the key side-chain residues surrounding the pocket are depicted in orange and white. White residues in the plane of the inhibitor are shown as white solids, and orange ball-and-stick residues (W229, Y183, and P95) project out of the plane.

tyl group in the complex. Of the three drugs studied, α-APA has its A wing highest up in the binding pocket where it is more distant from solvent molecules than is the A wing of the other drugs.

Among the major side-chain residues that show significant movement in proceeding from the starting RT/DNA structure to the final minimized complex with α-APA are Y181, Y188, W229, Y318. W229 is displaced upward (~3.8 Å) and Y181 and Y188 move upward by way of rotation (~70° and 116°, respectively) around their respective CA–CB bonds. If unliganded RT is taken as the starting structure, W229 is displaced ~4.5 Å and Y181 and Y188 are rotated by 188° and 128°, respectively. Comparison of these five side chains in the minimized RT/α-APA and RT/nevirapine complexes reveals that, although Y318 (RT/α-APA) and Y319 (RT/nevirapine) are in roughly the same position, there is significant variation (~1.3–1.75 Å) in the orientation of the other side-chain residues (Fig. 6). Aside from the Y318/Y319 switch, the greatest difference between the two complexes is in the position of W229. In the α-APA structure, the side chain is rotated about CB–CG ~180° and CG is displaced ~2.2 Å, compared with the structure where nevirapine is bound.

Examination of the interaction energies (Table 3) between α-APA and the protein side chains in our preferred α-APA/A orientation show that eight residues make significant contributions: Y188, Y181, K103, L100, V179, V106, W229, and K101, with the first four being the most important. Taken together, interactions with these eight residues accounts for over 67% of the total drug–protein interaction energy. The Y188 energy of −10 kcal/mol is the largest single residue interaction of all three drugs studied. Several nonaromatic, hydrophobic residues are important in the binding of α-APA. As in the nevirapine complex, L100 nests into the concave face of the butterfly, making contact with both wings. V106 meets the convex face of the α-APA B wing and the carboxamido carbonyl oxygen, whereas V179 contacts one bromine atom and interacts through its backbone carbonyl with the α-APA carboxamido N-*H* (N–O 3.63, H–O 2.79 Å). The large electrostatic component in the V179 binding energy suggests this latter interaction is substantial, though its geometry is less than ideal for a true hydrogen bond.

The drug–protein interactions again correlate with the mutant data for this compound (Pauwels et al., 1993; Ding et al., 1995b), which implicate Y188, Y181, and, to a lesser extent, K103 as important residues in α-APA binding. Although there is a substantial electrostatic component to the interaction with K103, the major contact is with the hydrocarbon portion of the side chain, CB, CG, and CE. RTs carrying the mutations Y318L or Y319L were both as susceptible to α-APA as the wild-type enzyme (Boyer & Hughes, unpubl. data), in agreement with relatively weak aromatic stacking with these residues and their low interaction energies (−1.75 and −0.09 kcal/mol, respectively). There is a significant interaction between the carboxamido N-*H* of α-APA and the backbone carbonyl oxygen of Y318 (O–H

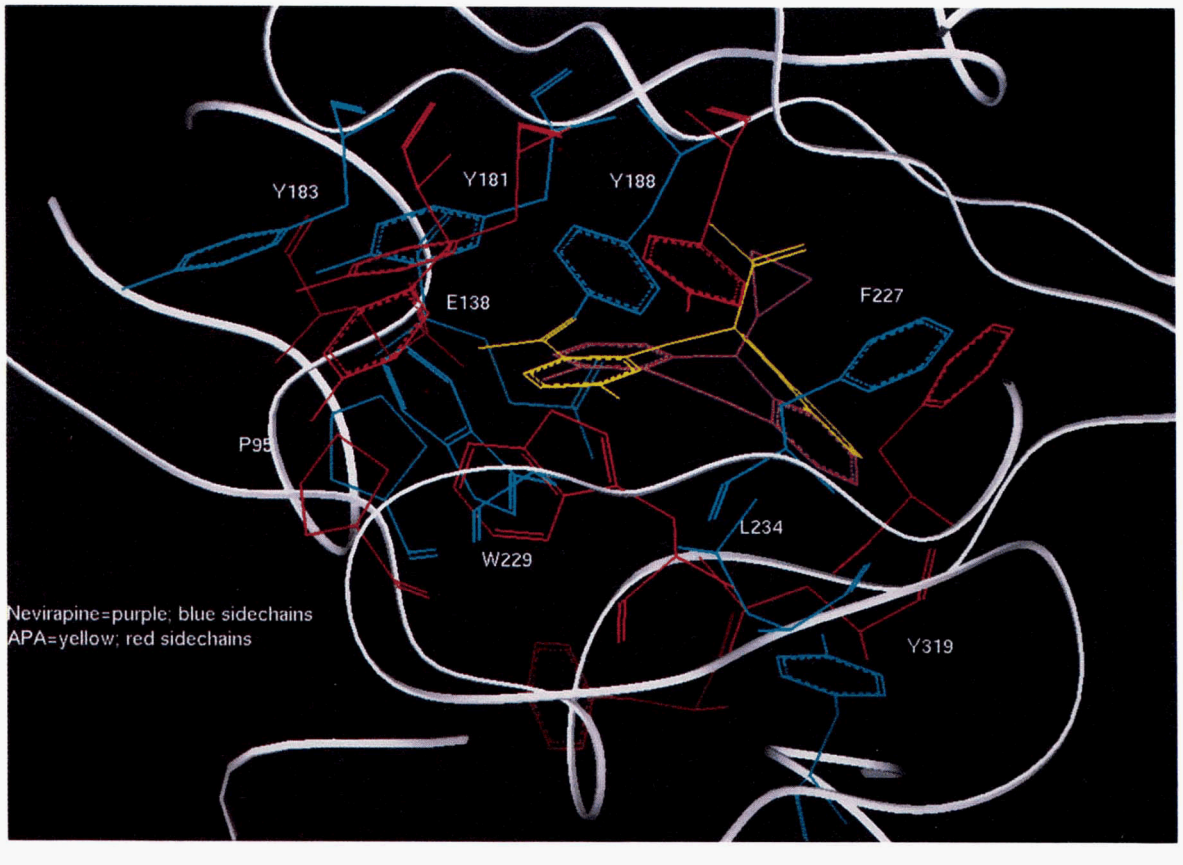

Fig. 6. Superposition of the α-APA and nevirapine-minimized structures showing differences in the position of key side-chain residues Y181, Y188, W229, P95, Y319, F227, and L234, surrounding the binding pocket. Nevirapine is shown in purple, with its key residues in blue, and α-APA is shown in orange with its side chains in red.

2.39 Å); however, this should not be markedly influenced by the Y318L mutation. The geometry of this interaction is atypical of hydrogen bonding. As in the case of nevirapine, the residue interaction energies for α-APA are greater in its preferred α-APA/A position than in the B orientation, with the exception of residues L100, G190, and L234.

Analysis of the aromatic interactions in the minimized RT/α-APA complex (Table 4) reveals π-stacking with side-chain residues Y181, Y318, Y188, and Y229. The first two interactions are of the parallel displaced type, whereas the latter two are tilted T, in agreement with the crystal structure (Ding et al., 1995b). Comparison of this structure with α-APA/B orientation reveals that the centroid distance between Y188 and the nearest drug aromatic ring is greater in the α-APA/B orientation (6.39 Å to the B ring) than in the α-APA/A orientation (5.32 Å to the A ring). This result correlates with the α-APA-Y188 interaction energy values of −10 kcal/mol (α-APA/A) versus −8.3 kcal/mol (α-APA/B) and clearly contributes to the preference for the α-APA/A orientation. The interactions with Y188, K103, and L101, all of which have large electrostatic components, constitute major differences between the α-APA/A and α-APA/B orientations.

TIBO

TIBO (R86183) was modeled in sites constructed from crystal structure data from each of the inhibitors complexed with RT. The results from these calculations are shown in Table 1. The binding energies of all of the possible drug orientations were more favorable in a site constructed from RT/TIBO coordinates than if either RT/nevirapine or RT/α-APA structural data was used in the calculation (−202 versus −76 or −97 kcal/mol). In the RT/TIBO site, the binding energy favored the T2/D orientation, which matches the position of the drug in the crystal structure (Ding et al., 1995a). (The binding energy data from the TIBO minimizations in the RT/nevirapine site also predicted the optimal orientation; the RT/α-APA site did not.) This inhibitor orientation was unexpected and is unique among the three drugs in that it does not place an aromatic wing of the inhibitor in the Y181/Y188 region.

The overall RMS value for protein backbone superposition of the initial and final complex structures was 0.47 Å. Only certain portions of the inhibitor were found to move during the minimization; the largest change was in the S atom position, which moved 1.8 Å. The C11 carbon atom (CH_3 *cis* to H) of the alkenyl side chain moved 0.6 Å, whereas the N2 atom (at the 5,7-ring junction) in the seven-membered ring was altered only by 0.23 Å from the initial (crystal structure) starting position. In calculations using the optimal TIBO-T2/D orientation, the inhibitor was found to form a good hydrogen bond (N-O distance = 2.88 Å, O-H distance = 1.96 Å) with a C-O-H angle of 170° to the backbone carbonyl oxygen atom of K101. This hydrogen bond was also reported in the crystal structure (Ding et al., 1995a).

The contributions to the total binding energy of each of the interactions accompanying complex formation are summarized in Table 2. As in the case of the other inhibitors, the intermolecular protein-solvent interaction makes the most favorable contribution to the total binding energy, followed by intramolecular protein and intermolecular drug-protein interactions. The complexed protein is considerably stabilized by solvation (−107.7 kcal/mol) and has assumed a more stable internal conformation than in the RT/DNA structure. On the basis of the protein alone, this conformation of RT is the most stable of all those measured in the present study. Stabilizing interactions between the drug and the protein (−51.18 kcal/mol) make a sizable contribution to the overall binding energy. The binding site residues once again can be seen to make close van der Waals contacts with the bound inhibitor (Fig. 7). As in the case of the other two drugs, the value for this latter interaction was similar to that of the final docking energy (−57 kcal/mol) and was greater than that of the other orientations (T1/D and T2/A) of the inhibitor. Thus, the drug-protein interaction values match the order of the final docking energies for all three drugs. There are two unfavorable energy terms associated with formation of the RT/TIBO complex. The drug itself adopts a slightly less favorable conformation in the complex ($\Delta E_{intradrug}$ = +2.75 kcal/mol). As with the other two drugs, there is a substantial cost associated with desolvation of the drug ($\Delta E_{interdrug\text{-}solvent}$ = +48.19 kcal/mol) in order to form the complex.

In the binding pocket region, the side-chain residues that move the most during the transition from RT/DNA to the RT/TIBO complex are Y181, Y188, W229, Y318, and Y319. W229 is displaced upward by 4.4 Å and Y181 and Y188 turn up 69° and 101°, respectively, as measured by rotation about their CA-CB bonds. In the lower part of the drug binding pocket, Y318 in RT/TIBO and RT/DNA occupy similar positions (displaced 0.5 Å) that are analogous to those seen in the α-APA complex. If unliganded RT is assumed to be the starting structure, W229 is displaced by 4.9°, whereas Y181 and Y188 are rotated by 117° and 113°, respectively. Those residues that make the closest contacts with TIBO are the same as in the other drug complexes. As was noted previously, however, the side chains appear to adjust to each specific inhibitor in a unique manner. Comparison of the positions of these side chains in the TIBO and α-APA complexes shows movement varying from approximately 0.4 Å for Y188 to 1.4 Å for W229. Deviation of these side-chain positions between the TIBO and nevirapine complexes is somewhat greater; for Y188 movement is about 1.0 Å, whereas for W229 it is 2.2 Å. In general, the side-chain positions appear to be more similar between the α-APA and TIBO structures than between either of these structures and the structure of the nevirapine complex. The orientations of both W229 and Y318 are quite similar in the structures of the TIBO and α-APA minimized complexes but differ substantially from those in the RT/nevirapine complex. With regard to backbone conformation, the superposition RMS value between α-APA and TIBO is 0.825 Å, whereas for TIBO and nevirapine it is 1.30 Å and for α-APA and nevirapine it is 1.37 Å.

Examination of the interaction energies between TIBO and the residues surrounding the binding pocket (Table 3) reveals that two residues, Y188 and L100, make relatively large contributions to the drug-protein interaction energy. Beyond these, a large number of other residues play a roughly similar, but lesser, role in binding: V106, L234, K101, W229, V179, Y181, K101, and G190. This pattern is different from the complexes with α-APA and nevirapine, where binding seems to be dominated by four to six strongly interacting residues. This is perhaps associated with the fact that, in TIBO, the wings are more flattened and the alkenyl side-chain wing is nonaromatic. The angle subtended by the two "wings" is ~140° in nevirapine, ~125° in α-APA, but ~165° in TIBO. Y188 makes the largest

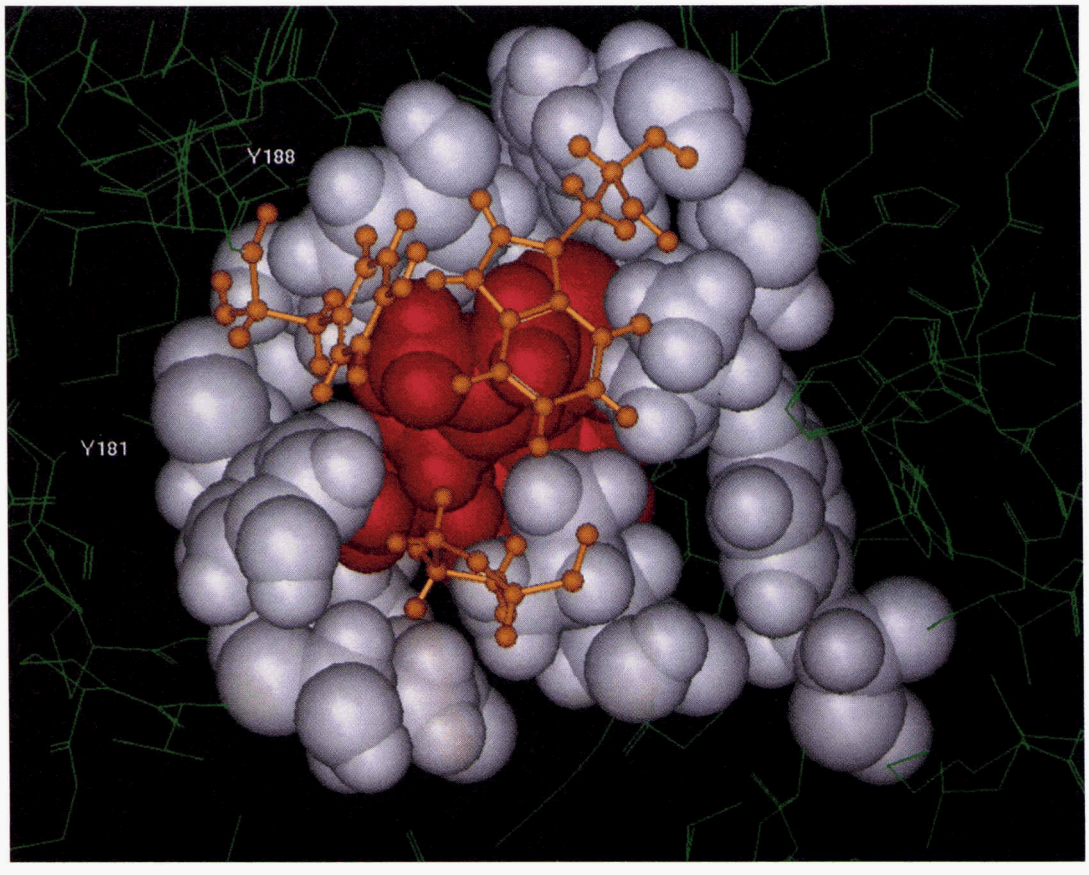

Fig. 7. Close-up view of the TIBO binding pocket, with a space-filling model of the drug shown in red. The van der Waals surface of the key side-chain residues surrounding the pocket are depicted in orange and white. White residues in the plane of the inhibitor are shown as white solids, and orange ball-and-stick residues (W229, Y183, and P95) project out of the plane.

contribution to the binding energy and interacts by way of van der Waals contacts between its side chain (CB and ring) and the alkenyl side chain of TIBO. As with the other complexes, interaction with nonpolar hydrophobic residues plays an important role in drug–protein binding. L100 lies in the concave face of the drug, but, because TIBO is much more flattened, contact is mainly with the alkenyl side chain and to a lesser extent, with the drug A ring. On the opposite side of the A ring, contact is made with V106. Through interactions with the 8-chloro group and the alkenyl side chain, L234 plays a more important role in TIBO binding than in the other drug complexes. Additional residues that interact with the alkenyl side chain are W229, V179, and Y181.

K101 and K103 are the only residues where electrostatic forces are dominant. In the case of K101, this is due to a hydrogen bond between the drug N-*H* and the backbone carbonyl oxygen. The N–O distance is 2.88 Å and the N–H–O angle is 150°. The geometry of this interaction is within the scope of a normal NH hydrogen bond to a carbonyl oxygen, with the hydrogen lying in the plane of the carbonyl group and bisecting the oxygen nonbonded pairs. The alkyl chain of K103 (specifically CG and CE) makes close van der Waals contact with the sulfur atom of TIBO. The large electrostatic component of the interaction with K103 is presumably due to the close proximity of the positively charged amino group to the TIBO sulfur atom.

The above results correlate with the mutational data for TIBO, which implicate L100, K103, Y181, Y188, and to a lesser extent, V106 (from p66) and E138 (from p51) (Boyer et al., 1994). Among the inhibitor orientations modeled, only TIBO-T2/D and α-APA/A showed any direct interaction with E138 (E = −1.63 or −2.06 kcal/mol, respectively). Although no mutant data for the effect of this residue on the binding of α-APA are available, it has been suggested (Ding et al., 1995b) that the orientation of this residue may affect the precise position of the inhibitor, as well as the side-chain position of Y181.

In the preferred T2/D orientation of TIBO, the interaction energies of Y188, V106, G190, and L234 (Table 3) are greater than those observed in the other two possible orientations. However, the energies of the other residues listed are greater in the other alternative positions than in T2/D. Because of this, the difference in drug–protein interaction energy among the various orientations of TIBO is significantly less (4.4 kcal/mol) than between the orientations of α-APA and nevirapine (10.8 and 9.5 kcal/mol, respectively).

Because TIBO has only one aromatic "wing," true π-stacking interactions in the TIBO-T2/D orientation are limited to Y318. Table 3, however, shows interaction with this residue to be weak (−1.56 kcal/mol). Although the D ring of TIBO is formally in a perpendicular orientation to the aromatic ring of Y318, the drug is substantially displaced and overlap between the π-clouds

is minimal. There are, however, significant interactions between the alkenyl side chain of TIBO and aromatic residues in the top of the binding pocket, specifically Y181, W229, and most notably Y188, as was described above. These interactions presumably involve the alkenyl methyl groups, although some degree of π–π overlap is possible with Y188 and W229.

Mechanism of nonnucleoside binding and inhibition in RT

It is not currently known if the nonnucleoside inhibitors in this study complex with unliganded RT and/or RT/DNA. In the absence of an inhibitor, the side chains of Y181 and Y188 in both RT/DNA (Jacobo-Molina et al., 1993) and unliganded RT (Esnouf et al., 1995; Rodgers et al., 1995) point into the hydrophobic core of the protein, and, therefore, the nonnucleoside binding pocket does not exist. It has been postulated (Rodgers et al., 1995) that the key event, which makes binding of the inhibitor possible, is the shift and rotation of the sheet formed by β12–14 (see Fig. 8). This allows W229 to move upward, withdrawing from the developing binding site. In turn, this motion creates room for the side chains of Y181 and Y188 to rotate upward to a position pointing toward the catalytic aspartic acid residues. As a result of these events, a hydrophobic pocket of sufficient volume to accommodate the inhibitor is created. A key question is what event triggers this sequence of motions? One possibility is contact between the inhibitor and the protein.

Both unliganded RT and RT/DNA contain a small surface depression comprised of residues L100, K101, K103, V179, and Y181 from p66 and E138 of p51, as suggested by Ding et al. (1995a). Although the binding pocket that is eventually created is itself hydrophobic, three of these residues are hydrophilic (K101, K103, and E138). Mutagenesis has shown that K103 is important in the binding of all three inhibitors. Although these mutagenesis data can be explained in terms of interactions between the drug and the protein in the final complex, similar interactions in the initial stages of the approach of the inhibitor toward the enzyme may also be quite important. The flexible and polar side chains of these residues may help in directing the inhibitor into the entrance of the pocket via electrostatic interactions, in part by replacing the original hydrogen bonds between the drug and the solvent. Any initial energy gains from such polar interactions with the inhibitors would be subsequently replaced by hydrogen bonds or other types of interactions with alternative residues as the inhibitor progresses deeper into the binding pocket. Inspection of the inhibitor–protein residue interaction energies in Table 3 reveals that for all three inhibitors, the values for L100 are quite negative. Although interactions with this residue are clearly important in the final complex, it is also possible it plays a significant attractive role in guiding the drugs into the pocket through hydrophobic interactions.

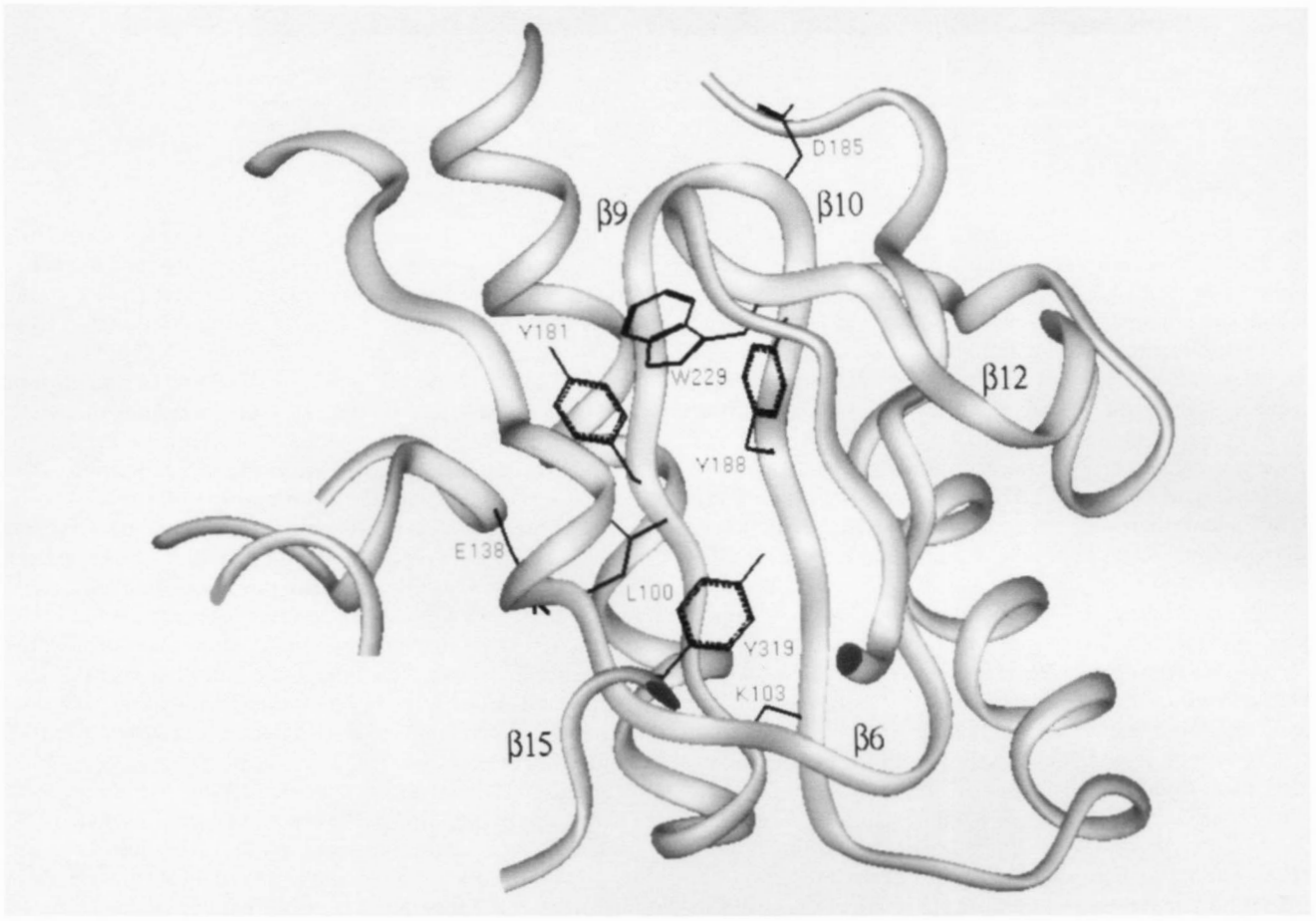

Fig. 8. Portions of the RT/nevirapine site with key side-chain residues and strands identified.

A significant portion of the aromatic ring of Y181 is exposed at the bottom of the surface depression, a feature that offers the potential for early $\pi-\pi$ interaction with the inhibitor. In unliganded RT, only one edge of Y181 is exposed to solvent. More significantly, however, in RT/DNA not only the edge, but also a significant portion of the aromatic π-cloud of Y181 is accessible to the solvent. This suggests complexation with RT/DNA may be the more favored pathway. The fact that our molecular orbital analysis was able to predict the efficacy of different inhibitors (as measured by EC_{50}'s) suggests that these types of $\pi-\pi$ aromatic interactions might also play a significant role in the initial approach of the drugs to the binding pocket. A test of this hypothesis would be to study changes in the strength of this interaction in response to modifications of the drug structure. Using the methods presented herein, one could evaluate both the classical mechanical (binding energy) and quantum mechanical (HOMO–LUMO) contributions to this interaction. If this hypothesis is correct, it provides an alternative, kinetic explanation for the ineffectiveness of nonnucleoside inhibitors against strains of the virus bearing nonaromatic mutations at residue 181.

As the solvated drug approaches the enzyme and proceeds to enter the binding region, most of the waters of solvation are lost. The few waters (1–2) that remain typically are located at the entrance to the pocket, forming a water bridge between the drug and one or two polar residues (E138, K103) at the solvent–protein interface. Ren et al. (1995) showed, in the case of nevirapine, that an additional water molecule can be trapped deeper in the pocket. Once the inhibitor is in place, the surface residues close down around the drug, effectively sealing the entrance to the pocket and preventing escape of the drug.

Preliminary computer modeling calculations for the approach of nevirapine to the surface of RT/DNA (and unliganded RT) were carried out in order to test the hypotheses presented above. Nevirapine was docked with its A ring in close proximity to Y181 and an energy minimization was conducted. The results of this calculation with RT/DNA showed movement of the drug (1.4 Å) toward its ultimate binding position, an upward displacement of W229 (0.7 Å), and an upward rotation of Y188 (14°). Although these changes are modest, they do mirror the early stages of drug binding as we have hypothesized and support the contention that contact between the drug and the protein surface depression initiates motions that lead to creation of the binding pocket.

Once the nonnucleoside inhibitors bind in the pocket, the results of modeling suggest a rather straightforward explanation for the mechanism by which these inhibitors interfere with the polymerase activity of RT through an allosteric effect. Upon formation of the ternary RT/nucleic acid duplex/dNTP complex, bond formation must occur between the free 3′-OH group on the primer strand and the α-phosphate of the dNTP. Thus, the distance between the primer grip and the dNTP binding site would be critical to the bond formation process. Amino acid residues G231 and D186 can be taken, respectively, as locants of these two sites on the protein (Patel et al., 1995). In all three complexes studied, these distances (G231:CA to D186:CG) increase dramatically (nevirapine, 12.56 Å; α-APA, 13.80 Å; and TIBO, 15.00 Å) in comparison with that observed in RT/DNA (9.33 Å). It is also interesting to note that the magnitude of this displacement is inversely related to the EC_{50} for each of the inhibitors. These data suggest that ability to impede the formation of the new sugar–phosphate linkage by displacement of the reactant binding sites may be an important factor in determining the effectiveness of a given inhibitor.

Implications for the design of better inhibitors

The evaluation of the interactions responsible for stabilizing the binding of nonnucleoside inhibitors complexed with RT provides valuable insight into potential applications directed toward the design of more effective drugs against AIDS. Our results show the differential adjustment of side-chain residues surrounding the binding pocket following binding of each inhibitor and imply that a single generic site will not suffice for molecular modeling studies, at least in the case where energy gradient minimizations are employed. The appropriate coordinate data for each inhibitor are needed to carry out reliable computer calculations. With the growing availability of relevant crystallographic data, it should now be possible to determine if the present method can be extended to the evaluation of different derivatives of a given drug, e.g., α-APA, with the ultimate goal being the design of a more effective inhibitor of HIV-1 RT.

Our results from the measurement of the interaction energies between the side-chain residues surrounding the binding pocket and the bound inhibitor (Table 3) provide information to guide those investigations. For example, close inspection of the van der Waals interactions between the side-chain residues and the inhibitors (Figs. 4, 5, 7) reveals that, although the side chains do adjust to close down around the drug, the protein is unable to fill all of the voids, and thus there is room for additional nonpolar, polar, or charged groups. Moreover, our conclusions suggest that modification of the inhibitor would result in adjustment of the proximate side-chain residues and could perhaps improve the interaction with residues such as L100, K101, K103, V106, or L234. Of key importance would be structural modifications designed to enhance interactions in the final complex between the drug and nonmutable residues, for example W229, and correspondingly diminish the importance of binding to mutable residues such as Y181 and Y188 in the final complex. Alterations of this type would address the crucial problem of the development of inhibitor-resistant mutants of HIV-1 RT.

Materials and methods

For enzymatic assays, a 6.82 μM solution of recombinant mutant reverse transcriptase p66 homodimer (0.90 mg/mL in 37.1 mM diethanolamine, 250 mM NaCl, and 5 mM dithiothreitol, pH 9.3) was used. The version used in these experiments contained the C280S mutation that has no measurable effect on enzymatic activity but increased long-term stability of the protein. The poly(rC):oligo$(dG)_{12-18}$ template primer and unlabeled dGTP-α-*S* (deoxyguanosine 5′-[α-thio]triphosphate) were from Pharmacia. Radiolabeled [^{35}S]deoxyguanosine 5′-(α-thio)triphosphate (specific activity of 1,200–1,300 Ci/mmol) was from New England Nuclear. For the assay, radiolabeled nucleotide was diluted with unlabeled nucleotide to yield a specific activity of 0.15 Ci/mmol. Nonidet P-40 was purchased from Sigma Chemical Co. Nevirapine (BI-RG-587) was the gift of Dr. Michael Currens, NCI-FCRDC. The dibrominated analog of α-APA (R95845), and the 8-chloro (R86183) and 9-chloro (R82913) TIBO compounds were kindly provided by Janssen Pharmaceutica.

Enzyme assay

Reaction mixtures contained 50 mM Tris, pH 8.3, 60 mM NaCl, 10 mM $MgCl_2$, 20 mM dithiothreitol, 0.05% Nonidet P-40, 6 mg/mL template primer, 35 μM nucleotide, and 34 nM enzyme in a total final volume of 50 μL. Inhibitors were added as solutions in dimethylsulfoxide such that the final dimethylsulfoxide concentration was 2.0% in all samples. Incubation mixtures were warmed to 37 °C, and reactions were initiated by the addition of enzyme. Following a 2-min incubation period at 37 °C, reactions were stopped by the addition of 100 μL of 10% trichloroacetic acid. The samples were kept at 0 °C for at least 30 min prior to filtration on Whatman Gf/C glass fiber filters. Total radiolabel incorporation was determined by liquid scintillation counting of the filters after drying. Inhibitors were tested over a range of 10 different concentrations and each concentration of a given inhibitor was determined in duplicate. Reported EC_{50} values are the mean of the results of three separate experiments. The assay conditions were chosen to maximize the maintenance of steady-state conditions throughout the incubation period. The average rate of nucleotide incorporation in control (uninhibited) samples was 4.48 ± 0.44 nM/s. This resulted in consumption of approximately 2.7% of the available sites on the template primer and 1.5% of the nucleotide.

Construction of mutant HIV-1 RTs

Variant HIV-1 RT mutants were constructed by *Bsp*M I cassette mutagenesis as described previously (Boyer et al., 1992). These mutants, which differ only at the designated sites of mutation, were used to evaluate differences in resistance to the nonnucleoside inhibitors compared to wild-type HIV-1 RT. Any differences in activity could be attributed directly to the specific mutation, because the mutants all have the same genetic background.

Computer modeling: Construction of the site

Modeling of the enzyme and inhibitor complexes was done with INSIGHT II (Biosym), with all calculations performed using the C Force Field (cff91) within Discover module mounted on a Cray YMP-8 supercomputer. The modeling calculations were based on the X-ray structure coordinates of RT complexed with nevirapine (Smerdon et al., 1994) and those of RT complexed with 2,6-dibromo-α-APA and 8-chloroTIBO (Ding et al., 1995a, 1995b). A modified site surrounding the inhibitor binding pocket was constructed for each complex from the respective enzyme coordinates and consisted of p51 subdomain residues 132–142, and residues 89–116, 156–211, 213–243, 265–271, 313–323, 346–351, and 380–384 from the p66 subdomain. These residues were selected using a distance criterion of ~20 Å from the inhibitor. Each of the eight strands of protein listed above was terminated on the C-terminal end with a methylamino group and on the N-terminal end with an acetyl group by altering (via deletion of atoms) the structure of the terminal residues. The pH of the site was set to 7.5, resulting in a total charge equal to zero; charged residues included Lys+, Arg+, Asp−, and Glu−. The hydrogens on each site were minimized prior to fitting the inhibitors into the binding pocket. In cases where the crystal structure resolution was inadequate to resolve side-chain positions of all the residues that were included in our model site, these side chains (not more than six per site) were changed from that reported (as alanines) and minimized in the absence of solvent prior to minimization of the site in solvent with a docked inhibitor.

Considering the structures in Figure 1 as "butterfly" shaped, one can assign the groups that constitute the aromatic wings in each (Ding et al., 1995a). For nevirapine, the two wings are the A and C rings. In α-APA, one wing is made up of the A ring and the acetyl group, and the other is the B ring. TIBO is different in that it has only one aromatic wing, consisting of the A ring. TIBO's second wing consists of simply the alkenyl group (designated D in the figure) attached to N(4). The overall shape of the drug and the binding pocket constrain the two aromatic wings of the drug to lie in different, i.e., upper and lower, portions of the binding pocket. Conceptually, the pocket can be divided into an upper region, which is proximal to the polymerase site, and a lower (distal) region. The inhibitors were initially modeled in the binding site based on the crystal structure position and geometry in their respective RT complexes. As a result, for both nevirapine and α-APA the A ring was oriented toward Y181 and Y188 (see Fig. 8), whereas for TIBO, the D moiety was directed toward these residues. Alternative orientations were also considered; e.g., nevirapine with its C ring positioned close to these residues. In addition, to determine if a single generic site would have predictive value, calculations were performed with a given drug placed in the binding pocket of sites constructed from crystal coordinates derived from complexes with a different drug. Particularly in the case of these latter "hybrid" calculations, any initial steric interactions between the drug and protein were reduced using the Docking module of Insight II until the initial docking energy was below 500 kcal/mol. In calculations for all of the sites, solvent was added by means of the default cvff waterbox to create a 6-Å layer of water molecules surrounding first the site and then the inhibitor. In our model, the higher cvff forcefield partial charges for water O (−0.820) and H (0.410) lead to a better approximation of solvent hydrogen bonding behavior than do those of the cff91 forcefield (−0.798 and 0.399, respectively). All other parameters for water are the same in both forcefields.

To allow flexibility in the vicinity of the inhibitor and yet retain conformity with the omitted portions of p66 and p51, the site was divided into a primary and a secondary layer. Residues comprising the primary layer were chosen using a 10-Å cutoff distance from the inhibitor; this layer included p66 residues 94–111, 176–193, 223–237, 318 or 319, and p51 residues 136–138. The secondary layer consisted of the remaining residues: 89–93, 112–175, 194–222, 238–317 (or 318), 319 (or 320)–323, 346–351, 380–384 from p66, and 132–135, and 139–142 from p51. Minimizations of the enzyme–inhibitor complexes were carried out in three stages. Each stage consisted of a steep descent minimization for 200 iterations, followed by a conjugate gradient minimization until the RMS was less than or equal to 0.001 Å (nonbonded cutoff = 100 Å in all calculations). In the first stage, the solvent was minimized holding both the drug and protein fully constrained. Second, the complex was minimized with the backbone of the primary protein layer surrounding the binding pocket constrained and all atoms in the secondary layer fully constrained. In the third stage, the backbone of the primary layer was also released so that both the drug and those protein residues within 10 Å were free to move, whereas the secondary layer was still held frozen. In the nevirapine calculations Y319 was not constrained, whereas in the α-APA and TIBO minimizations the calculations were carried out with Y318 free, due to

a switch in position of Y318 and Y319 between the nevirapine crystal structure (Kohlstaedt et al., 1992; Smerdon et al., 1994) and those of α-APA and TIBO (Ding et al., 1995a). It should be noted that other recent crystal data (Ren et al., 1995), which were not available at the time these calculations were undertaken, suggest that Y318 points into the binding pocket in all RT/inhibitor complexes, including the nevirapine complex. Our study does not attempt to resolve this issue and the modeling relies only upon the fact that one of these two tyrosine side chains is present in the pocket.

It should be stressed that the above-described model is just that, a model. For practical reasons, a number of assumptions and approximations were made in designing this computational method. Truncation of the protein at ~20 Å neglects structural changes that occur more distant from the inhibitor binding site, changes that we assume would have a relatively less important effect on the binding of each inhibitor. The use of a 6-Å layer of water was chosen to obtain a reasonable approximation of solvation effects, whereas at the same time limiting the system to a manageable number (ca. 1,250 per complex) of solvent molecules. The choice of an energy minimization approach clearly leaves open the possibility of encountering local minima. Although alternative computational approaches, such as Monte Carlo-based dynamics, would likely have lessened this issue, the extended computational time involved in these methods made them impractical given our desire to design a relatively rapid method of evaluation.

Computer modeling: Binding energy analysis

The binding energy for the formation of each RT/drug complex is the change in strain energy associated with the following equilibrium, where D is the free drug, P is the free protein, and D'-P' is the resultant complex (primes indicate altered conformation, dash indicates a nonbonded interaction).

$$D + P \rightleftharpoons D'P'.$$

The fundamental underlying assumption of our method is that there exists the following biochemical/thermodynamic relationship:

$$EC_{50} * K_{inhib} * e^{-BE}, \quad (1)$$

where K_{inhib} is the equilibrium constant for the complexation reaction shown in Equation 1. Implicit in the above relationship, which is strictly correct only for $e^{-\Delta G}$, is the assumption that entropic changes are approximately equal for the different RT/inhibitor complexes; hence comparison of binding energies is based on the assumption $\Delta\Delta G \approx \Delta\Delta H \approx \Delta BE$. Binding energies were calculated by subtracting products from reactants according to the standard formula:

$$BE_{total} = E_{[D'-P']} - (E_{[D]} + E_{[P]}). \quad (2)$$

In our calculation of the binding energies, the starting protein (P) was chosen to be RT/DNA, for reasons that will be discussed later. For all species containing the protein (i.e., P and D'-P'), after minimization in solvent, a further single point energy calculation (0 iteration) with both Y318 and Y319 included in the unconstrained primary layer was performed in order to remove artificial energy variation between the different complexes and the constraints used in their particular minimization. (Constraining a residue in a single point calculation has the effect of neglecting intramolecular energy terms for that residue.) All energy values were then corrected to remove the energy of the solvent molecules. To accomplish this for each solvated species, a single point energy calculation on its respective solvent object was performed and this energy was subtracted from that of the minimized solvated species. The resultant solvent-corrected energies (italicized), $E_{[D]}$, $E_{[P]}$, and $E_{[D'-P']}$, were then used in Equation 2 to obtain the binding energy for the complex.

The energy changes (ΔE) in the various molecular interactions that occur when the free drug and protein are converted to the drug–protein complex were also calculated. In the overall complexation reaction, solvation could play an important role, and thus it is more precise to view the above equilibrium in terms of solvated species:

$$D\text{-}S_1 + P\text{-}S_2 \rightleftharpoons D'\text{-}P'\text{-}S_3 \quad (3)$$

Contributions to the final binding energy for this conversion result from changes in the following: the intramolecular energy of the drug (ΔE_{intraD}), the intramolecular energy of the protein site (ΔE_{intraP}), intermolecular energy resulting from interaction between the drug and the protein in the complex ($E_{interD'-P'}$, note: there is no Δ, because it is logical to assume that there is no interaction on the reactant side of the equilibrium), and intermolecular energy (solvation energy) from interaction between each species and the solvent ($\Delta E_{interD-S}$, $\Delta E_{interP-S}$). It should also be noted that this approach treats solvation of the complex as two separate terms, $E_{interD'-S3}$ and $E_{interP'-S3}$. The binding energy then is given by:

$$BE_{total} = \Delta E_{intraD} + \Delta E_{intraP} + \Delta E_{interD-S} + \Delta E_{interP-S} + E_{interD'-P'}, \quad (4)$$

where

$$\Delta E_{intraD} = E_{D'} - E_D, \quad (5)$$

$$\Delta E_{intraP} = E_{P'} - E_P, \quad (6)$$

$$\Delta E_{interD-S} = [E_{D'-S3} - (E_{D'} + E_{S3})] - [E_{D-S1} - (E_D + E_{S1})], \quad (7)$$

$$\Delta E_{interP-S} = [E_{P'-S3} - (E_{P'} + E_{S3})] - [E_{P-S2} - (E_P + E_{S2})], \quad (8)$$

$$E_{interD'-P'} = [E_{D'-P'} - (E_{D'} + E_{P'})]. \quad (9)$$

To clarify the calculation of certain terms in Equations 7–9, it should be pointed out that Discover permits the calculation of the energy of any object or an assembly of two (or more) objects. The energy of intermolecular interaction (e.g., $E_{interD'-P'}$)

between any two assembled objects is obtained from the difference between the energy of the assembly (e.g., $E_{D'-P'}$) and the sum of the energies of the two individual objects (e.g., $E_{D'} + E_{P'}$). As above, all energies involving the protein were determined using a single point calculation with both Y318 and Y319 unconstrained in the primary layer. It should also be noted that, although the designation of some of the terms in Equation 2 are the same as those in Equations 5-9, the former are solvent-corrected and the latter are not. We have used italics to emphasize this distinction. Final BE_{total} values calculated using Equations 2 and 4 are identical, indicating that the latter method of analysis correctly accounts for all of the necessary energy terms in the complexation reaction.

As has been described above, the construction of this model and the associated calculations include a number of assumptions and approximations. The final binding energies, therefore, should only be interpreted as qualitative measures of the relative complexation efficiency of the various inhibitors studied.

Computer modeling: Miscellaneous calculations

The relative magnitude of the interactions between the drug and individual residues in the binding site of the final complex were determined using the Docking module within the Insight II package. Solvent-accessible surface areas (Connolly, 1983) of each protein were measured also using Insight II. For the complexed proteins, these areas include the binding pocket, which is not truly accessible to the solvent due to the presence of the inhibitor.

In order to assess possible quantum mechanical contributions to aromatic interactions, calculations of the energies and locations of the highest occupied and unoccupied molecular orbitals of the crystal structure conformations of the inhibitors at the Restricted Hartree-Fock (RHF) 3-21G* and 6-31G* levels of theory were carried out using the Gaussian 92 computer program mounted on a Cray YMP-8 supercomputer. The RHF/3-21G* calculations were performed, in part, to permit approximation of RHF/6-31G* energies for α-APA R95845 (a dibromo compound), because the larger basis set lacks functions for the treatment of bromine atoms. Semi-empirical AM1 quantum mechanical calculations, using the program Spartan 3.1 (Wavefunction, Inc.), on amino acid trimers or tetramers of the same sequence as that surrounding aromatic protein residues (Y181, Y188, and Y318/Y319) in the binding pocket, were performed to evaluate qualitatively the location and energies of the protein molecular orbitals. A simple β-sheet backbone conformation was used, and these fragments were terminated as *N*-acetyl and *N*-methylamino amides.

Centroid distances to evaluate possible aromatic stacking interactions were calculated by means of a program (written in True Basic) that reads the Cartesian coordinate files generated by Discover. The program employed the Euler method for determining centroids for the heavy atoms of the side-chain aromatic moieties and intercentroid distances between these and each aromatic moiety of the drug molecule. Because of various possible $\pi-\pi$ interaction modes, W229 centroids were determined independently for the five- and six-membered rings, and for the entire 10-atom aromatic system. For drug molecules, centroids were calculated for each individual aromatic ring. In the case of TIBO, the centroid double bond of the alkenyl side chain was used for distance determination. Assignment of the type of aromatic $\pi-\pi$ interaction was based on two criteria, the intercentroid distance and the interplanar angle for the two aromatic groups. Distances of 4.0 ± 0.5 Å and angles of ≤ 45° corresponded to parallel displaced, whereas distances of 5.5 ± 0.5 Å and angles of >45° were categorized as perpendicular or tilted-T. For perpendicular interactions, the long axis (defined by a line passing through any pair of ring carbon atoms bearing a 1,4 relationship) of one aromatic ring is perpendicular to the plane of the other. In the tilted-T, the long axis is parallel to the plane of the second ring. For interactions to be significant, it was assumed that the two rings must be oriented such that at least one hydrogen atom (or methyl group) attached to a drug must lie within the aromatic π-cloud of the protein side chain.

Acknowledgments

We thank David Rodgers and Stephen Harrison for providing the unliganded HIV-1 RT coordinates prior to general distribution and Chris Tantillo of CABM for helpful discussions. In addition, we acknowledge the Frederick Biomedical Supercomputing Center of the Frederick Cancer Research and Development Center for access to the Cray-YMP computer. Research was sponsored by the National Cancer Institute, DHHS, under contract no. N01 CO-46000 with ABL. R.H.S. was supported in part by the National Science Foundation (CHE-9215925). CABM research was supported by the Janssen Research Foundation and NIH grants AI 27690 and AI 36144. The contents of this publication do not necessarily reflect the views or policies of the Department of Health and Human Services, nor does mention of trade names, commercial products, or organizations imply endorsement by the US government. By acceptance of this article, the publisher or recipient acknowledges the right of the U.S. Government and its agents and contractors to retain a nonexclusive royalty-free license in and to any copyright covering the article.

References

Baba M, De Clercq E, Tanaka H, Ubasawa M, Takashima H, Sekiya K, Nitta I, Umezu K, Nakashima H, Mori S, Shigeta S, Walker R, Miyasak T. 1990. Potent and selective inhibition of human immunodeficiency virus type 1 (HIV-1) by 5-ethyl-6-phenylthiouracil derivatives through their interactions with the HIV-1 reverse transcriptase. *Proc Natl Acad Sci USA 88*:2356-2360.

Bacolla A, Shih CK, Rose JM, Piras G, Warren TC, Grygon CA, Ingraham RH, Cousins RC, Greenwood DJ, Richman D, Cheng YC, Griffin JA. 1993. Amino acid substitutions in HIV-1 reverse transcriptase with corresponding residues from HIV-2. *J Biol Chem 268*:16571-16577.

Balzarini J, Karlsson A, Perez-Perez MJ, Vrang L, Walbers J, Zhang H, Oberg B, Vandamme AM, Camarasa MJ, De Clercq E. 1993. HIV-1 specific reverse transcriptase inhibitors show differential activity against HIV-1 mutant strains containing different amino acid substitutions in the reverse transcriptase. *Virology 192*:246-253.

Boyer PL, Ding J, Arnold E, Hughes SH. 1994. Subunit specificity of mutations that confer resistance to nonnucleoside inhibitors in human immunodeficiency virus type 1 reverse transcriptase. *Antimicrob Agents Chemother 38*:1909-1914.

Boyer PL, Ferris AL, Hughes SH. 1992. Cassette mutagenesis of the reverse transcriptase of human immunodeficiency virus type 1. *J Virol 66*: 1031-1039.

Burley SK, Petsko GA. 1985. Aromatic-aromatic interactions: A mechanism of protein structure stabilization. *Science 229*:23-28.

Burley SK, Petsko GA. 1988. Weakly polar interactions in proteins. *Adv Protein Chem 39*:125-192.

Connolly ML. 1983. Solvent-accessible surfaces of proteins and nucleic acids. *Science 221*:709-713.

Debyser Z, De Vreese K, Knops-Gerrits PP, Baekelandt V, Bhikhabbai R, Strandberg B, Pauwels R, Anne J, Desmyter J, De Clercq E. 1993. Kinetics of different human immunodeficiency virus type 1 reverse transcriptases resistant to human immunodeficiency virus type 1-specific reverse transcriptase inhibitors. *Mol Pharmacol 43*:521-526.

Debyser Z, Pauwels R, Andries K, Desmyter J, Kukla M, Janssen PAJ, De Clercq E. 1991. An antiviral target on reverse transcriptase of human

immunodeficiency virus type 1 revealed by tetrahydroimidazo-[4,5,1-*jk*] [1,4] benzodiazepin-2(1*H*)-one and -thione derivatives. *Proc Natl Acad Sci USA 88*:1451-1455.

De Clerq E. 1992. HIV inhibitors targeted at the reverse transcriptase. *AIDS Res Human Retroviruses 8*:119-134.

DiMarzo-Veronese F, Copeland TD, DeVico AL, Rahman R, Oroszlan S, Gallo RC, Sarngadharan MC. 1986. Characterization of the highly immunogenic p66/p51 as the reverse transcriptase of HTLV-III/LAV. *Science 231*:1289-1291.

Ding J, Das K, Moereels H, Koymans L, Andries K, Janssen PAJ, Hughes SH, Arnold E. 1995a. Structure of HIV-1 RT/TIBO R86183 complex reveals remarkable similarity in the binding of diverse nonnucleoside inhibitors. *Nature Struct Biol 2*:407-415.

Ding J, Das K, Tantillo C, Zhang W, Clark AD Jr, Jessen S, Lu X, Hsiou Y, Jacobo-Molina A, Andries K, Pauwels R, Moereels H, Koymans L, Janssen PAJ, Smith RH Jr, Koepke MBK, Michejda CJ, Hughes SH, Arnold E. 1995b. Structure of HIV-1 reverse transcriptase in a complex with the non-nucleoside inhibitor α-APA R95845 at 2.8 Å resolution. *Structure 3*:365-379.

Esnouf R, Ren J, Ross C, Jones Y, Stammers D, Stuart D. 1995. Mechanism of inhibition of HIV-1 reverse transcriptase by non-nucleoside inhibitors. *Struct Biol 2*:303-308.

Fukui K, Fujimoto H. 1967. The stereoselection rule for electrocyclic interactions. *Bull Chem Soc Jpn 40*:2018-2021.

Goff SP. 1990. Retroviral reverse transcriptase: Synthesis, structure, and function. *J Acquired Immune Defic Syndr 3*:817-831.

Hargrave KD, Proudfoot JR, Grozinger KG, Cullen E, Kapadia SR, Patel UR, Fuchs VU, Maudlin SC, Vitous J, Behnke ML, Klunder JM, Pal K, Skiles JW, McNeil DW, Rose JM, Chow GC, Skoog MT, Wu JC, Schmidt G, Engel WW, Eberlein WG, Saboe TD, Campbell SJ, Rosenthal AS, Adams J. 1991. Non non-nucleoside inhibitors of HIV-1 reverse transcriptase. 1. Tricyclic pyridobenzo- and dipyridodiazepinones. *J Med Chem 34*:2231-2241.

Holloway MK, Wai JM, Halgren TA, Fitzgerald PMD, Vacca JP, Dorsey BD, Levin RB, Thompson WJ, Chen LJ, deSolms SJ, Gaffin N, Ghosh AK, Giuliani EA, Graham SL, Guare JP, Hungate RW, Lyle TA, Sanders WM, Tucker TJ, Wiggins M, Wiscount CA, Woltersdorf OW, Young SD, Darke PL, Zugay JA. 1995. A priori prediction of activity for HIV-1 protease inhibitors employing energy minimization in the active site. *J Med Chem 38*:305-317.

Hunter CA, Sanders JKM. 1990. The nature of π-π interactions. *J Am Chem Soc 112*:5525-5534.

Hunter CA, Singh J, Thorton JM. 1991. π-π Interactions: The geometry and energetics of phenylalanine-phenylalanine interactions in proteins. *J Mol Biol 218*:837-846.

Jacobo-Molina A, Ding J, Nanni RG, Clark AD Jr, Lu X, Tantillo C, Williams RL, Kamer G, Ferris AL, Clark P, Hizi A, Hughes SH, Arnold E. 1993. Crystal structure of human immunodeficiency virus type 1 reverse transcriptase complexed with double-stranded DNA at 3.0 Å resolution shows bent DNA. *Proc Natl Acad Sci USA 90*:6320-6324.

Jacques PS, Wöhrl BM, Ottman M, Darlix JL, LeGrice SFJ. 1994. Mutating the "primer grip" of p66 HIV-1 reverse transcriptase implicates tryptophan-229 in template-primer utilization. *J Biol Chem 269*:26472-26478.

Jäger J, Smerdon S, Wang J, Boisvert DC, Steitz TA. 1994. Comparison of three different crystal forms shows HIV-1 reverse transcriptase displays an internal swivel motion. *Structure 2*:869-876.

Jorgensen WL, Severance DL. 1990. Aromatic-aromatic interactions: Free energy profiles for the benzene dimer in water, chloroform, and liquid benzene. *J Am Chem Soc 112*:4768-4774.

Kohlstaedt LA, Wang J, Friedman JM, Rice PA, Steitz TA. 1992. Crystal structure at 3.5 Å resolution of HIV-1 reverse transcriptase complexed with an inhibitor. *Science 256*:1783-1790.

Kopp EB, Miglietla JJ, Shrutkowski AG, Shih CK, Grob PM, Skoog MT. 1991. Steady state kinetics and inhibition of HIV-1 reverse transcriptase by a non-nucleoside dipyridodiazepinone, BI-RG-587, using a heteropolymer template. *Nucleic Acids Res 19*:3035-3039.

Larder BA. 1992. 3'-Azido-3'-deoxythymidine resistance suppressed by a mutation conferring human immunodeficiency virus type 1 resistance to nonnucleoside reverse transcriptase inhibitors. *Antimicrob Agents Chemother 36*:2664-2669.

Larder BA. 1993. Inhibitors of HIV reverse transcriptase as antiviral agents and drug resistance. In: Skalka AM, Goff SP, eds. *Reverse transcriptase*. Cold Spring Harbor, New York: Cold Spring Harbor Monograph Series, Cold Spring Harbor Laboratory Press. pp 205-222.

Larder BA, Kemp SD. 1990. Multiple mutations in HIV-1 reverse transcriptase confer high-level resistance to zidovudine (AZT). *Science 246*:1155-1158.

Mellors JW, Dutschman GE, Im G-j, Tramontano E, Winkler SR, Cheng YC. 1992a. Rapid emergence of HIV-1 resistance to non-nucleoside inhibitors of reverse transcriptase. *Antiviral Res 17 S1*:48.

Mellors JW, Dutschman GE, Im G-j, Tramontano E, Winkler SR, Cheng YC. 1992b. In vitro selection and molecular characterization of human immunodeficiency virus-1 resistant to non-nucleoside inhibitors of reverse transcriptase. *Mol Pharmacol 41*:446-451.

Mitsuya H, Yarchoan R, Broder S. 1990. Molecular targets for AIDS therapy. *Science 249*:1533-1544.

Nanni RG, Ding J, Jacobo-Molina A, Hughes SH, Arnold E. 1993. Review of HIV-1 reverse transcriptase three-dimensional structure: Implications for drug design. *Perspect Drug Discovery Des 1*:129-150.

Nunberg JH, Schlief WA, Boots EJ, O'Brien JA, Quintero JC, Hoffman JM, Emini EA, Goldman ME. 1991. Viral resistance to human immunodeficiency virus type 1-specific pyridinone reverse transcriptase inhibitors. *J Virol 65*:4887-4892.

Palladino DEH, Hopkins JL, Ingraham RH, Warren TC, Kapadia SR, Van Moffaert GJ, Grob PM, Stevenson JM, Cohen K. 1994. High-performance liquid chromatography and photoaffinity crosslinking to explore the binding environment of nevirapine to reverse transcriptase of human immunodeficiency virus type-1. *J Chromatogr A 676*:99-112.

Patel PH, Jacobo-Molina A, Ding J, Tantillo C, Clark AD, Raag R, Nanni RG, Hughes SH, Arnold E. 1995. Insights into DNA polymerization mechanisms from structure and function analysis of HIV-1 reverse transcriptase. *Biochemistry 34*:5351-5363.

Pauwels R, Andries K, Debyser Z, Van Daele P, Schols D, Stoffels P, De Vreese K, Woestenborghs R, Vandamme AM, Janssen CGM, Anne J, Cauwenbergh G, Desmyter J, Heykants J, Janssen MAC, De Clercq E, Janssen PAJ. 1993. Potent and highly selective human immunodeficiency virus type 1 (HIV-1) inhibition by a series of α-anilinophenylacetamide derivatives targeted at HIV-1 reverse transcriptase. *Proc Natl Acad Sci USA 90*:1711-1715.

Pauwels R, Andries K, Desmyter J, Schols D, Kukla MJ, Breslin HJ, Raeymaekers A, Van Gelder J, Woestenborghs R, Heykants J, Schellekens K, Janssen MAC, De Clercq E, Janssen PAJ. 1990. Potent and selective inhibition of HIV-1 replication in vitro by a novel series of TIBO derivatives. *Nature (Lond) 343*:470-474.

Raag R, Nanni RG, Clark AD Jr, Ding J, Jacobo-Molina A, Lu X, Tantillo C, Hughes SH, Arnold E. 1994. 3.0 Å Crystal structure of HIV-1 reverse transcriptase without dsDNA reveals large-scale motion of p66 thumb subdomain. *Am Crystallogr Assoc Mtg Abstr, Ser 2 18*:44.

Ren J, Esnouf R, Garman E, Somers D, Ross C, Kirby I, Keeling J, Darby G, Jones Y, Stuart D, Stammers D. 1995. High resolution structures of HIV-1 RT from four RT-inhibitor complexes. *Struct Biol 2*:293-302.

Richman D, Shih CK, Lowy I, Rose J, Prodanovich P, Goff S, Griffin J. 1991. Human immunodeficiency type 1 mutants resistant to non-nucleoside inhibitors of reverse transcriptase arise in tissue culture. *Proc Natl Acad Sci USA 88*:11241-11245.

Richman DD. 1993. Resistance of clinical isolates of human immunodeficiency virus to antiretroviral agents. *Antimicrob Agents Chemother 37*:1207-1213.

Rodgers DW, Gamblin SJ, Harris BA, Ray S, Culp JS, Hellmig B, Woolf DJ, Debouck C, Harrison SC. 1995. The structure of unliganded reverse transcriptase from the human immunodeficiency virus type 1. *Proc Natl Acad Sci USA 92*:1222-1226.

Romero DL, Busso M, Tan CK, Reusser F, Palmer JR, Poppe SM, Aristoff PA, Downey KM, So AG, Resnick L, Tarpley WG. 1991. Nonnucleoside reverse transcriptase inhibitors that potently and specifically block human immunodeficiency type 1 replication. *Proc Natl Acad Sci USA 88*:8806-8810.

Sardana VV, Emini EA, Gotlib L, Graham DJ, Lineberger DW, Long WJ, Schlabach AJ, Wolfgang J, Condra JH. 1992. Functional analysis of HIV-1 reverse transcriptase amino acids involved in resistance to multiple nonnucleoside inhibitors. *J Biol Chem 267*:17526-17530.

Schafer W, Friebe WG, Leinhart H, Mertens A, Poll T, von der Saal W, Zilch H, Nuber B, Ziegler ML. 1993. Inhibitors of HIV-1 reverse transcriptase: Molecular modeling and X-ray structure investigations. *J Med Chem 36*:726-732.

Schinazi RF. 1993. Competitive inhibitors of human immunodeficiency virus reverse transcriptase. *Perspect Drug Discovery Des 1*:151-180.

Schlief WA, Emini EA, Rhodes A, Titus DL, Gotlib L, Condra JH, Byrnes VW. 1992. Development and analysis of human immunodeficiency virus type 1 resistant to HIV-1 specific pyridinone reverse transcriptase inhibitors. *J Cell Biochem* (Suppl 16E):87.

Smerdon SJ, Jager J, Wang J, Kohlstaedt LA, Chirino AJ, Friedman JM, Rice PA, Steitz TA. 1994. Structure of the binding site for nonnucleoside inhibitors of the reverse transcriptase of human immunodeficiency type 1. *Proc Natl Acad Sci USA 91*:3911-3915.

Spence RA, Kati WM, Anderson KS, Johnson KA. 1995. Mechanism of in-

hibition of HIV-1 reverse transcriptase by nonnucleoside inhibitors. *Science 267*:988–993.

St. Clair MH, Martin JL, Tudor-Williams G, Back MC, Vavro CL, King DM, Kellam P, Kemp SD, Larder BA. 1991. Resistance to ddI and sensitivity to AZT induced by a mutation in HIV-1 reverse transcriptase. *Science 253*:1557–1559.

Tantillo C, Ding J, Jacobo-Molina A, Nanni RG, Boyer PL, Hughes SH, Pauwels R, Andries K, Janssen PAJ, Arnold E. 1994. Locations of anti-AIDS drug binding sites and resistance mutants in the three-dimensional structure of HIV-1 reverse transcriptase: Implications for mechanisms of drug inhibition and resistance. *J Mol Biol 243*:369–387.

Taylor R, Kennard O, Versichel W. 1985. Geometry of the N-H···O=C hydrogen bond. 1. Lone pair directionality. *J Am Chem Soc 105*:5761–5766.